



**HAL**  
open science

## A two-dimensional method for a family of dispersive shallow water model

Nora Aïssiouene, Marie-Odile Bristeau, Edwige Godlewski, Anne Mangeney, Carlos Parés, Jacques Sainte-Marie

► **To cite this version:**

Nora Aïssiouene, Marie-Odile Bristeau, Edwige Godlewski, Anne Mangeney, Carlos Parés, et al.. A two-dimensional method for a family of dispersive shallow water model. 2019. hal-01632522v2

**HAL Id: hal-01632522**

**<https://hal.science/hal-01632522v2>**

Preprint submitted on 25 Mar 2019 (v2), last revised 13 May 2020 (v5)

**HAL** is a multi-disciplinary open access archive for the deposit and dissemination of scientific research documents, whether they are published or not. The documents may come from teaching and research institutions in France or abroad, or from public or private research centers.

L'archive ouverte pluridisciplinaire **HAL**, est destinée au dépôt et à la diffusion de documents scientifiques de niveau recherche, publiés ou non, émanant des établissements d'enseignement et de recherche français ou étrangers, des laboratoires publics ou privés.

# A two-dimensional method for a family of dispersive shallow water models

Nora Aïssiouene<sup>1</sup>, Marie-Odile Bristeau<sup>2,3</sup>, Edwige Godlewski<sup>2,3</sup>,  
Anne Mangeney<sup>2,3,4</sup>, Carlos Parés<sup>5</sup>, and Jacques Sainte-Marie<sup>2,3</sup>

March 24, 2019

## Abstract

We propose a numerical method for a family of two-dimensional dispersive shallow water systems with topography. The considered models consist in shallow water approximations – without the hydrostatic assumption – of the incompressible Euler system with free surface. Hence, the studied models appear as extensions of the classical shallow water system enriched with dispersive terms. The model formulation motivates to use a prediction-correction scheme for its numerical approximation. The prediction part leads to solving a classical shallow water system with topography while the correction part leads to solving an elliptic-type problem. The numerical approximation of the considered dispersive models in the two-dimensional case over unstructured meshes is described, it requires to combine finite volume and finite element techniques. A special emphasis is given to the formulation and the numerical resolution of the correction step (variational formulation, inf-sup condition, boundary conditions,...). The numerical procedure is confronted with analytical and experimental test cases. Finally, an application to a real tsunami case is given.

**Keywords:** shallow water flows, dispersive effects, prediction-correction scheme, combined finite volume / finite element technique, dispersive wave propagation, tsunami propagation

## Contents

<b>1</b>	<b>Introduction</b>	<b>2</b>
<b>2</b>	<b>A class of dispersive models</b>	<b>4</b>
2.1	Model formulation . . . . .	4
2.2	The boundary conditions . . . . .	6

---

<sup>1</sup>Sorbonne Université, Institut Carnot Smiles, 4 Place Jussieu, F-75252 Paris cedex 05, Nora.Aïssiouene@upmc.fr

<sup>2</sup>Inria Paris, 2 rue Simone Iff, CS 42112, 75589 Paris Cedex 12, France

<sup>3</sup>Sorbonne Université, Université Paris-Diderot SPC, CNRS, Laboratoire Jacques-Louis Lions, LJLL, F-75005 Paris

<sup>4</sup>Univ. Paris Diderot, Sorbonne Paris Cité, Institut de Physique du Globe de Paris, Seismology Group, 1 rue Jussieu, Paris F-75005, France

<sup>5</sup>EDANYA, Universidad de Málaga, Campus de Teatinos s/n, 29080 Málaga, Spain

2.3	A justification of the model . . . . .	6
2.3.1	The Euler system . . . . .	7
2.3.2	An approximation of the Euler system . . . . .	7
2.3.3	The value of $\gamma$ . . . . .	9
<b>3</b>	<b>Time and space discretizations</b>	<b>10</b>
3.1	Prediction - correction scheme . . . . .	10
3.2	Space discretization . . . . .	11
3.3	Finite volume scheme for the prediction part . . . . .	12
3.4	The mixed problem . . . . .	13
3.4.1	Compatible boundary conditions . . . . .	14
3.4.2	Slip boundary conditions . . . . .	14
3.4.3	The variationnall formulation . . . . .	14
3.4.4	The inf-sup condition . . . . .	17
<b>4</b>	<b>Finite element approximations for the mixed problem</b>	<b>17</b>
4.1	The $P_1/P_1$ approximation . . . . .	18
4.2	A $P_1$ -iso $P_2/P_1$ approximation . . . . .	21
<b>5</b>	<b>Numerical algorithm</b>	<b>23</b>
5.1	Iterative methods . . . . .	23
5.2	Wet-dry interface . . . . .	25
5.3	An improved time scheme . . . . .	26
<b>6</b>	<b>Numerical validation</b>	<b>26</b>
6.1	A solitary wave . . . . .	26
6.2	A periodic analytical solution with wet-dry interfaces . . . . .	28
6.3	Dingemans experiments - effect of the choice of $\gamma$ . . . . .	31
6.4	Application to the 2014 Iquique earthquake, Chile . . . . .	35
<b>7</b>	<b>Conclusion</b>	<b>40</b>
<b>A</b>	<b>Equivalence with the Green-Naghdi system</b>	<b>46</b>

# 1 Introduction

Mathematical models for free surface flows are widely studied but their analysis and numerical approximation remains a challenging issue. The incompressible Navier-Stokes system with free surface being very difficult to study, it is often replaced by the classical shallow water equations [9]. But these equations rely on the hydrostatic assumption and hence when the vertical acceleration of the fluid can no longer be neglected, the shallow water system fails to represent dispersive effects e.g. in the context of wave propagation [32, 10].

Many shallow water type models taking into consideration the dispersive effects are available, see [34, 11, 12, 47, 46, 20, 19], the list being non-exhaustive. In this paper, we introduce a family of dispersive models depending on a parameter and where only first order derivatives appear. For a given value of the parameter we obtain the dispersive model proposed by some of the authors [19, 2] and for another value of the parameter the studied model corresponds

to the Green-Naghdi model [34, 4, 13, 21, 25] up to some small error terms involving the bathymetry gradient.

The non linear shallow water model with topography is an hyperbolic system with source term, which has been extensively studied and the literature provides efficient algorithms for this model, see [16, 44, 45] for analysis results and [33, 43, 15, 6, 7] for numerical methods. Since non-hydrostatic models are no longer hyperbolic, it is necessary to propose new numerical algorithms and there is a strong need for methods able to capture dispersion with a good accuracy and able to deal with real situations. Several approaches have been proposed to solve these models, especially in one dimension or in two dimensions with a structured grid (see [23, 13, 21, 28, 42]). A discretization with a discontinuous Galerkin method has been proposed in [25] to treat the dispersive part, and more recently, A. Duran and F. Marche performed an hybrid method [26] for the two-dimensional Green-Naghdi model. The same model is considered in [30] with combined finite volume / finite element on unstructured meshes.

Compared to most of existing techniques where the non-hydrostatic part of the pressure is eliminated – leading to third order derivative terms – we consider a formulation with only first order derivatives as initially proposed in [19]. This strategy leads to a non-hydrostatic pressure governed by an elliptic type equation as in the Chorin-Teman decomposition technique applied for the classical incompressible Euler system [49]. More precisely, the elliptic part of the system has the form of a Sturm-Liouville type equation and admits several formulations depending on the boundary conditions to be applied.

The aim of this paper is to provide, for this family of two-dimensional dispersive models, a stable and robust numerical method coupling finite volume and finite element strategies and able to simulate real cases where the topography can be complex. Therefore, the space discretization is performed over unstructured meshes.

The strong points of the paper are

- to consider a model formulation with only first order derivatives and with a duality relation between the pressure gradient and the divergence free condition similar to the one available for the classical incompressible Euler system,
- the numerical analysis of the elliptic equations governing the non-hydrostatic pressure (inf-sup condition),
- to propose a numerical scheme able to deal with wet/dry interfaces,
- the numerical treatment of the boundary conditions facilitated by the model structure and the time splitting,
- the convergence order of the method evaluated using several analytical solutions,
- the numerical procedure confronted with several test cases of wave propagation including a tsunami propagation.

The paper is organized as follows. In the next section, we present the family of dispersive models and its derivation from the full Euler system. Section 3 is devoted to the formulation of the Chorin-Teman approach (prediction-correction scheme) in the studied context, we mainly focus on the correction step consisting in the resolution of a mixed problem (velocity-pressure). In Section 4, we propose two approximation spaces ( $P_1/P_1$  and  $P_1$ -iso $P_2/P_1$ ) for the

finite element scheme applied to the mixed problem. Finally, we validate the implementations using comparisons with analytical solutions, and then we apply the method to an earthquake generated tsunami and compare the simulation results to field measurements.

## 2 A class of dispersive models

In this section, the family of 2d shallow water dispersive models studied in this paper is presented. First its formulation where only first order derivatives appear is given then we propose a justification of the family of models by the means of a depth averaging of the incompressible Euler with free surface and a suitable choice for the velocity and pressure fields.

### 2.1 Model formulation

We consider the family of 2d shallow water dispersive models written under the form

$$\frac{\partial H}{\partial t} + \frac{\partial(Hu)}{\partial x} + \frac{\partial(Hv)}{\partial y} = 0, \quad (1)$$

$$\frac{\partial(Hu)}{\partial t} + \frac{\partial}{\partial x} \left( Hu^2 + \frac{g}{2}H^2 + Hp \right) + \frac{\partial(Huv)}{\partial y} = -(gH + \gamma p) \frac{\partial z_b}{\partial x}, \quad (2)$$

$$\frac{\partial(Hv)}{\partial t} + \frac{\partial(Huv)}{\partial x} + \frac{\partial}{\partial y} \left( Hv^2 + \frac{g}{2}H^2 + Hp \right) = -(gH + \gamma p) \frac{\partial z_b}{\partial y}, \quad (3)$$

$$\frac{\partial(Hw)}{\partial t} + \frac{\partial(Huw)}{\partial x} + \frac{\partial(Hvw)}{\partial y} = \gamma p, \quad (4)$$

$$\gamma w = -H \frac{\partial u}{\partial x} + \gamma u \frac{\partial z_b}{\partial x} - H \frac{\partial v}{\partial y} + \gamma v \frac{\partial z_b}{\partial y}, \quad (5)$$

where  $\mathbf{u}(\mathbf{x}, t) = (u, v, w)^T$  is the velocity of the fluid,  $p$  is the non-hydrostatic part of the fluid pressure, the total pressure is given by  $p_{tot} = gH/2 + p$  and  $g$  represents the gravity acceleration.  $\gamma \in \mathbb{R}$  is a parameter, its value will be discussed in paragraph 2.3.

We consider the model (1)-(5) is written for a two-dimensional domain  $\Omega \subset \mathbb{R}^2$  delimited by the boundary  $\Gamma = \Gamma_{in} \cup \Gamma_{out} \cup \Gamma_s$  as described in Fig. 1a. We denote  $\mathbf{x} = (x, y)$ . The topography profile is  $z_b(\mathbf{x})$  and the free surface is defined by

$$\eta(\mathbf{x}, t) := H(\mathbf{x}, t) + z_b(\mathbf{x}),$$

$H(\mathbf{x}, t)$  being the water depth.

For smooth solutions, the system (1)-(5) satisfies the following energy balance

$$\frac{\partial E}{\partial t} + \nabla_0 \cdot \left( \mathbf{U} \left( E + \frac{g}{2}H^2 + Hp \right) \right) = 0, \quad (6)$$

with  $\nabla_0 = \left( \frac{\partial}{\partial x}, \frac{\partial}{\partial y}, 0 \right)^T$  and  $E = H|\mathbf{u}|^2/2 + g(\eta^2 - z_b^2)/2$ .

Compared to the classical formulation of the Green-Naghdi system, the formulation (1)-(5) has two main advantages

- the writing of the model exhibits a structure that is very similar to the full incompressible Euler system with free surface. Hence, Eq. (1) stands for the mass conservation, Eqs. (2)-(4) are a vertically averaged version of the momentum equations along  $x$ ,  $y$  and  $z$  of the full Euler system and Eq. (5) is a shallow water version of the divergence free condition. These similarities allow to adapt for the dispersive shallow water model numerical techniques initially proposed for the full Euler system.
- The system (1)-(5) contains only first order derivatives and their numerical treatment is easier than third order derivatives appearing in most of the dispersive shallow water models studied in the litterature Peregrine [47], Nwogu [46], BBM [12], Green-Naghdi [34]...

The system (1)-(5) defines a family  $\{\mathcal{M}_\gamma\}$  of dispersive models written in the more condensed form

$$\frac{\partial H}{\partial t} + \nabla_0 \cdot (H\mathbf{u}) = 0, \quad (7)$$

$$\frac{\partial(H\mathbf{u})}{\partial t} + \nabla_0 \cdot (H\mathbf{u} \otimes \mathbf{u}) + \nabla_0 \cdot \left(\frac{g}{2}H^2\right) + \nabla_{sw}^\gamma p = -gH\nabla_0(z_b), \quad (8)$$

$$\operatorname{div}_{sw}^\gamma(\mathbf{u}) = 0, \quad (9)$$

where

$$\nabla_{sw}^\gamma f = \begin{pmatrix} H \frac{\partial f}{\partial x} + f \frac{\partial \zeta}{\partial x} \\ H \frac{\partial f}{\partial y} + f \frac{\partial \zeta}{\partial y} \\ -\gamma f \end{pmatrix}, \quad (10)$$

$$\operatorname{div}_{sw}^\gamma(\mathbf{w}) = \frac{\partial(Hw_1)}{\partial x} + \frac{\partial(Hw_2)}{\partial y} - w_1 \frac{\partial \zeta}{\partial x} - w_2 \frac{\partial \zeta}{\partial y} + \gamma w_3, \quad (11)$$

for  $\mathbf{w} = (w_1, w_2, w_3)^T$  and

$$\zeta = H + \gamma z_b. \quad (12)$$

Whereas  $\zeta$  depends on  $\gamma$ , for the sake of simplicity, we have adopted a simplified notation and  $\zeta_\gamma$  is replaced by  $\zeta$ .

A key point is that the operators  $\operatorname{div}_{sw}^\gamma$  and  $\nabla_{sw}^\gamma$  satisfy the duality relation (analogous to the duality relation between the gradient and divergence operator for the full incompressible Euler system, see Eq. (29))

$$\int_{\Omega} \nabla_{sw}^\gamma(f) \cdot \mathbf{w} d\mathbf{x} = - \int_{\Omega} \operatorname{div}_{sw}^\gamma(\mathbf{w}) f d\mathbf{x} + \int_{\Gamma} H f \mathbf{w} \cdot \mathbf{n} ds, \quad (13)$$

where  $f$  and  $\mathbf{w}$  belong to suitable function spaces that will be precised later and  $\mathbf{n} = (n_x, n_y, 0)^T$  is the outward unit normal vector to the boundary  $\Gamma$ , see Fig. 1. This property is crucial for the algorithm presented in the following since we will consider a mixed problem in velocity/pressure (see Section 3.4), which will lead, at the numerical level, to having an operator for the pressure and its adjoint for the velocity.

## 2.2 The boundary conditions

The set of equations (7)-(9) is completed with the following boundary conditions. We are considering a channel with an inlet  $\Gamma_{in}$  and an outlet  $\Gamma_{out}$  and we impose specific conditions on each of them. The inflow is imposed by a given discharge  $\mathbf{q}_g(\mathbf{x}, t)$  on  $\Gamma_{in}$ , and a water depth  $h_g(\mathbf{x}, t)$  is imposed on  $\Gamma_{out}$ . Finally, we prescribe slip boundary conditions for the velocity at the walls of the channel  $\Gamma_s$ . Hence we have

$$H\mathbf{u}(\mathbf{x}, t) = \mathbf{q}_g(\mathbf{x}, t), \quad \text{on } \Gamma_{in}, \quad (14)$$

$$H(\mathbf{x}, t) = h_g(\mathbf{x}, t), \quad \text{on } \Gamma_{out}, \quad (15)$$

$$\mathbf{u}(\mathbf{x}, t) \cdot \mathbf{n} = 0, \quad \text{on } \Gamma_s. \quad (16)$$

Notice that we can replace the prescribed water depth at the outflow by a free outflow consisting in imposing a Neumann boundary condition over the elevation

$$\nabla_0 H \cdot \mathbf{n} = 0, \quad \text{on } \Gamma_{out}.$$

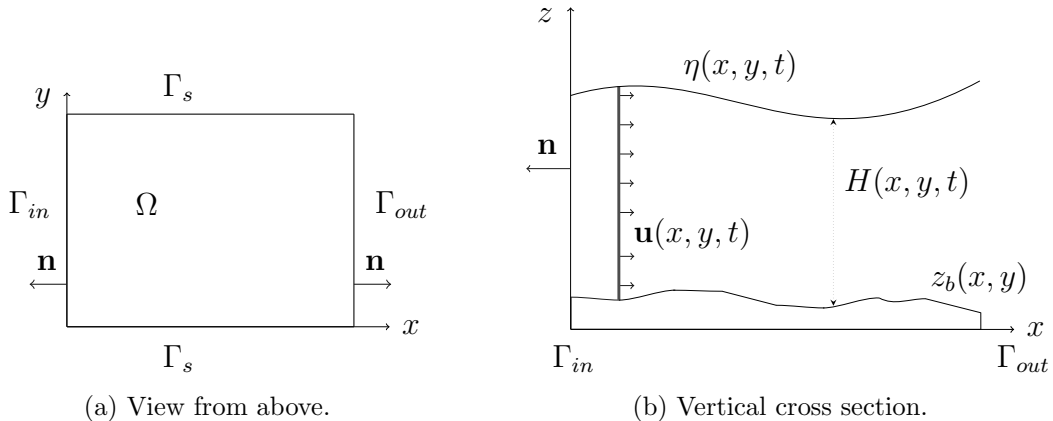


Figure 1: Model domain and notations.

## 2.3 A justification of the model

Dispersive models are often obtained using an asymptotic expansion of the Euler or Navier-Stokes system coupled with physical assumptions concerning the hydrodynamic regime. For shallow water flows, dispersive models are extensions of the classical shallow water system [31].

Particular choices of the parameter  $\gamma$  correspond to two dispersive models studied in the literature. More precisely,  $\gamma = 3/2$  leads to the Green-Naghdi model [34] whereas  $\gamma = 2$  leads to the model described in [19]. The complexity of the Euler system, able to represent many regimes from wave propagation to advection dominated flows, explains why many dispersive shallow water models have been proposed, see the references given in Section 1.

In this paragraph, we propose a unified approach consisting in an approximation of the depth averaged Euler system and allowing to recover various dispersive shallow water models,

see especially paragraph 2.3.2 and remark 2.2. But it is important to notice that the approximation process of the Euler system we propose is an *a posteriori* justification of the models  $\mathcal{M}_\gamma$  and cannot be considered as a modeling strategy.

### 2.3.1 The Euler system

The three-dimensional incompressible Euler system describing a free surface gravitational flow moving over a bottom topography  $z_b(\mathbf{x})$  writes

$$\nabla \cdot \mathbf{V} = 0, \quad (17)$$

$$\frac{\partial \mathbf{V}}{\partial t} + \nabla \cdot (\mathbf{V} \otimes \mathbf{V}) + \nabla \tilde{p} = -\mathbf{g}, \quad (18)$$

where  $\mathbf{V}(x, y, z, t) = (u_1, u_2, u_3)^T$  is the velocity,  $\tilde{p}$  is the fluid pressure and  $\mathbf{g} = (0, 0, g)^T$  represents the gravity forces. The quantity  $\nabla$  denotes  $\nabla = \left( \frac{\partial}{\partial x}, \frac{\partial}{\partial y}, \frac{\partial}{\partial z} \right)^T$ .

We consider a free surface flow, therefore we assume

$$z_b(\mathbf{x}) \leq z \leq \eta(\mathbf{x}, t) := H(\mathbf{x}, t) + z_b(\mathbf{x}).$$

The system (17)-(18) is completed with boundary conditions.

At the free surface, the kinematic boundary condition is

$$\frac{\partial \eta}{\partial t} + u_{1,s} \frac{\partial \eta}{\partial x} + u_{2,s} \frac{\partial \eta}{\partial y} - u_{3,s} = 0, \quad (19)$$

whereas at the bottom we have the non-penetration condition

$$u_{1,b} \frac{\partial z_b}{\partial x} + u_{2,b} \frac{\partial z_b}{\partial y} - u_{3,b} = 0, \quad (20)$$

where the subscript  $s$  (resp.  $b$ ) denotes the value of the considered quantity at the free surface (resp. at the bottom).

The dynamic boundary condition at the free surface is given by

$$\tilde{p}_s = \tilde{p}(\mathbf{x}, \eta, t) = p^a(\mathbf{x}, t), \quad (21)$$

where  $p^a$  mimics the role of the atmospheric pressure. Throughout this paper, we assume  $p^a(\mathbf{x}, t) = p_0^a = cst$ .

### 2.3.2 An approximation of the Euler system

For free surface flows, the vertical direction plays a particular role since it corresponds to the direction of the gravity. Moreover the fluid domain is thin in this direction. It is easy to see that a depth averaging of the Euler system (17)-(18) completed with the boundary conditions (19)-(21) leads to (see [31, Lemma 2.1])

$$\frac{\partial H}{\partial t} + \nabla_{x,y} \cdot \int_{z_b}^{\eta} \mathbf{v} dz = 0, \quad (22)$$

$$\frac{\partial}{\partial t} \int_{z_b}^{\eta} \mathbf{v} dz + \nabla_{x,y} \cdot \int_{z_b}^{\eta} \mathbf{v} \otimes \mathbf{v} dz + \nabla_{x,y} \int_{z_b}^{\eta} \tilde{p} dz = \tilde{p}(\mathbf{x}, z_b(\mathbf{x}), t) \nabla_{x,y} z_b, \quad (23)$$



$$\frac{\partial}{\partial t} \int_{z_b}^{\eta} u_3 dz + \nabla_{x,y} \cdot \int_{z_b}^{\eta} u_3 \mathbf{v} dz = \tilde{p}(\mathbf{x}, z_b(\mathbf{x}), t) - gH, \quad (24)$$

completed with (17) and with  $\mathbf{v} = (u_1, u_2)$ .

And the following proposition holds.

**Proposition 2.1** *A depth averaging of the incompressible Euler system with free surface (17)-(21) completed with a suitable approximation of the velocity field  $\mathbf{V}$  and of the pressure  $\tilde{p}$  in Eqs. (22)-(24) gives the model (1)-(5).*

**Proof of prop. 2.1** *Considering Eqs. (17),(22)-(24) it remains to choose the approximations for the variables  $\mathbf{V}$  and  $\tilde{p}$ . In order to be consistent with the shallow water assumption we choose for the horizontal velocities*

$$u_1(\mathbf{x}, z, t) = u(\mathbf{x}, t), \quad u_2(\mathbf{x}, z, t) = v(\mathbf{x}, t). \quad (25)$$

*It remains to choose approximations for the velocity  $u_3$  and for the pressure  $\tilde{p}$ .*

*Let us consider two families of functions  $\psi_\gamma = \psi_\gamma(z)$  and  $\varphi_\gamma = \varphi_\gamma(z)$  satisfying*

$$\begin{aligned} \int_0^1 \psi_\gamma(z) dz &= 1, \\ \psi_\gamma(1) &= \gamma, \\ \psi_\gamma(0) &= 0, \\ \int_0^1 \varphi_\gamma(z) \frac{\partial \psi_\gamma}{\partial z} dz &= \gamma. \end{aligned} \quad (26)$$

*Many choices are possible for  $\psi_\gamma$  and  $\varphi_\gamma$ , we exhibit two possible choices for  $\psi_\gamma$ , namely*

$$\begin{aligned} \psi_\gamma(z) &= 3(\gamma - 2)z^2 + 2(3 - \gamma)z \quad \text{for } \gamma \in \mathbb{R}, \\ \psi_\gamma(z) &= \gamma z^{\gamma-1}, \quad \text{for } \gamma \geq 1, \end{aligned}$$

*and for  $\varphi_\gamma$  a possible choice is*

$$\varphi_\gamma(z) = 1 - \frac{\mu\gamma}{2} + \mu\psi_\gamma(z).$$

*for any  $\mu \in \mathbb{R}$ . Now we define*

$$\tilde{p}(\mathbf{x}, z, t) = p_0^a + g(\eta - z) + \psi_\gamma \left( \frac{\eta - z}{H} \right) p(\mathbf{x}, t), \quad (27)$$

$$u_3(\mathbf{x}, z, t) = \varphi_\gamma \left( \frac{\eta - z}{H} \right) w(\mathbf{x}, t), \quad (28)$$

*meaning  $\psi_\gamma((\eta - z)/H)p(\mathbf{x}, t)$  corresponds to the non-hydrostatic part of the pressure. Because of the chosen approximation for  $\tilde{p}$  coupled with (26), the boundary condition (21) is satisfied.*

*And with the choices (25)-(28), Eqs. (2)-(4) exactly correspond to (23)-(24).*

For the incompressible Euler system (17)-(18), the duality relation between the velocity  $\mathbf{V}$  and the pressure  $\tilde{p}$  given by

$$\int_{\Omega \times [z_b, \eta]} \mathbf{V} \cdot \nabla \tilde{p} d\omega dz = \int_{\partial(\Omega \times [z_b, \eta])} \tilde{p} \mathbf{V} \cdot \mathbf{n} ds - \int_{\Omega \times [z_b, \eta]} \tilde{p} \nabla \cdot \mathbf{V} d\omega dz, \quad (29)$$

is a crucial point (notice that in Eq. (29),  $\mathbf{n}$  is the unit outward normal to the domain  $\Omega \times [z_b, \eta]$ ). Because of the choices (25)-(28), it comes

$$\int_{\Omega \times [z_b, \eta]} \tilde{p} \nabla \cdot \mathbf{V} d\omega dz = \int_{\Omega \times [z_b, \eta]} p \psi_\gamma \left( \frac{\eta - z}{H} \right) \nabla \cdot \mathbf{V} d\omega dz,$$

and we remark that

$$\int_{z_b}^{\eta} \psi_\gamma \left( \frac{\eta - z}{H} \right) \nabla \cdot \mathbf{V} dz = 0,$$

corresponds to Eq. (5). Notice that because of the properties of  $\psi_\gamma$  and  $\varphi_\gamma$  an analogous version of the duality relation (29) holds for the model (1)-(4), see Eq. (13). ■

**Remark 2.1** Instead of considering the approximation (25) where the velocities is supposed to be constant along the vertical axis, a piecewise constant approximation along the vertical axis can be considered (see [29]) and leading to a set of 2d equations approximating the 3d Euler system with free surface.

### 2.3.3 The value of $\gamma$

For  $\gamma = 3/2$ , the model (1)-(5) corresponds, up to small error terms, to the Green-Naghdi model [34] studied e.g. in [14, 40], this equivalence is proved in Appendix A. In the context of wave propagation i.e. with flat bottom and assuming the water depth has the form

$$H = H_0 + f(kx - \omega t),$$

with  $H_0 = cst$ ,  $f(\cdot) \ll H_0$ , it is easy to see that the linear dispersion relation of the model  $\mathbf{M}_\gamma$  is given by

$$\frac{\omega}{k} = \sqrt{gH_0} \left( 1 + \frac{(kH_0)^2}{2\gamma} \right)^{-1/2},$$

corresponding for  $\gamma = 3/2$  in the context of large wavelength ( $H_0 k \ll 1$ ) and up to  $\mathcal{O}((H_0 k)^4)$  terms, to the classical Airy wave dispersion relation.

The choice  $\gamma = 2$  corresponds to the model proposed and studied in 1d by some of the authors in [19, 2]. The model  $\mathcal{M}_2$  is more adapted to advection dominated flows. Indeed we can exhibit analytical solutions for the full Euler system that are also solutions of the model  $\mathcal{M}_\gamma$  only for  $\gamma = 2$ , see remark 6.1. Thus the model  $\mathcal{M}_\gamma$  for  $\gamma = 2$  shares common analytical solutions with the full Euler system.

But for the numerical analysis part that is the core of this paper, the authors do not want to single out one value of  $\gamma$  or another but propose a framework valid for the whole family of models.

**Remark 2.2** Notice that approximations and/or linearizations in the dispersive terms of  $\mathcal{M}_\gamma$  allow to recover other dispersive models such as Peregrine [47].

Indeed, considering a linearized version of  $\mathcal{M}_\gamma$  with  $\gamma = 3/2$  (where  $H = H_0 + h$ ,  $H_0 = cst$ ,  $h \ll H_0$ ,  $uv \ll 1$ ,  $uw \ll 1$ ) and a flat bottom gives

$$\frac{\partial H}{\partial t} + \frac{\partial(Hu)}{\partial x} + \frac{\partial(Hv)}{\partial y} = 0, \quad (30)$$

$$\frac{\partial u}{\partial t} + u \frac{\partial u}{\partial x} + v \frac{\partial u}{\partial y} + g \frac{\partial H}{\partial x} + \frac{\partial p}{\partial x} = 0, \quad (31)$$

$$\frac{\partial v}{\partial t} + u \frac{\partial v}{\partial x} + v \frac{\partial v}{\partial y} + g \frac{\partial H}{\partial y} + \frac{\partial p}{\partial y} = 0, \quad (32)$$

$$H_0 \frac{\partial w}{\partial t} = \gamma p, \quad (33)$$

$$\gamma w = -H_0 \frac{\partial u}{\partial x} - H_0 \frac{\partial v}{\partial y}. \quad (34)$$

Then, substituting Eq. (34) in Eq. (33) gives the expression of the pressure  $p$ . And inserting the obtained expression for  $p$  in Eqs.(31),(32) gives the Peregrine model [47].

### 3 Time and space discretizations

The time splitting strategy based on a Chorin-Temam projection-correction scheme (see [22, 49, 35, 36]) and the space discretization are first presented in this section. Then the correction step is studied.

#### 3.1 Prediction - correction scheme

The prediction-correction method is widely used to approximate the Navier-Stokes equations and is based on a time-splitting scheme. At each time step, the problem is decomposed into two steps. In the first one, we use a finite volume method to solve the hyperbolic part leading to a predicted state which does not satisfy the divergence free constraint. During the second step, we update the predicted state so that the divergence free constraint (9) is satisfied.

Let us introduce the notations

$$X = \begin{pmatrix} H \\ Hu \\ Hv \\ Hw \end{pmatrix}, \quad F(X) = \begin{pmatrix} Hu & Hv \\ Hu^2 + \frac{g}{2}H^2 & Huv \\ Huv & Hv^2 + \frac{g}{2}H^2 \\ Huv & Hvw \end{pmatrix},$$

and

$$S(X) = \begin{pmatrix} 0 \\ -gH \frac{\partial z_b}{\partial x} \\ -gH \frac{\partial z_b}{\partial y} \\ 0 \end{pmatrix}, \quad R = \begin{pmatrix} 0 \\ \nabla_{sw}^\gamma p \end{pmatrix}.$$

Then, the system (7)-(9) can be written under the form

$$\frac{\partial X}{\partial t} + \nabla_{x,y} \cdot F(X) + R = S(X), \quad (35)$$

$$\operatorname{div}_{sw}^{\gamma}(\mathbf{u}) = 0, \quad (36)$$

with  $\nabla_{x,y} = \left(\frac{\partial}{\partial x}, \frac{\partial}{\partial y}\right)^T$ .

We set  $t^0$  the initial time and  $t^{n+1} = t^n + \Delta t^n$  where  $\Delta t^n$  satisfies a stability condition (CFL) precised later and the state  $X^n$  will denote an approximation of  $X(t^n)$ . For each time step, we consider an intermediate state which will be denoted with the superscript  $n+1/2$ . So the first step leads to solving the hyperbolic system with the topography source term – that is exactly the classical shallow water system – in order to get the state  $X^{n+1/2} = (H^{n+1/2}, (Hu)^{n+1/2}, (Hv)^{n+1/2}, (Hw)^{n+1/2})^T$ . Finally, the semi-discretization in time can be summarized in the following steps

$$X^{n+1/2} = X^n - \Delta t^n \nabla_{x,y} \cdot F(X^n) + \Delta t^n S(X^n), \quad (37)$$

$$X^{n+1} = X^{n+1/2} - \Delta t^n R^{n+1}, \quad (38)$$

$$\operatorname{div}_{sw}^{\gamma} \mathbf{u}^{n+1} = 0. \quad (39)$$

Equation (38) allows us to correct the predicted value  $X^{n+1/2}$  in order to obtain a state which satisfies the divergence free condition (39). The equation satisfied by the pressure is then an elliptic equation which is obtained by applying the shallow water divergence operator  $\operatorname{div}_{sw}^{\gamma}$  to Eq. (38) and reads

$$\operatorname{div}_{sw}^{\gamma} \left( \frac{\nabla_{sw}^{\gamma} p^{n+1}}{H^{n+1}} \right) = \frac{1}{\Delta t^n} \operatorname{div}_{sw}^{\gamma} \left( \frac{(H\mathbf{u})^{n+1/2}}{H^{n+1/2}} \right). \quad (40)$$

Once the pressure has been determined by the elliptic equation (40), the correction step (38) gives the final step  $X^{n+1}$ .

In this paper, we briefly describe the step (37) in paragraph 3.3 but we will focus on the second step of the scheme, namely Eqs. (38)-(39) discretized by a finite element method. Therefore, we will consider the state  $X^{n+1/2}$  as a given state and the state  $X^{n+1}$  as the unknown. The operator  $\operatorname{div}_{sw}^{\gamma} \left( \frac{\nabla_{sw}^{\gamma}}{H} \right)$  is a shallow water version of the Laplacian operator and is denoted by  $\Delta_{sw}^{\gamma}$ , using (10),(11) its expression is given by

$$\Delta_{sw}^{\gamma} p = \nabla_{x,y} \cdot (H \nabla_{x,y} p) + \left( \Delta_{x,y} \zeta - \frac{1}{H} \left( \left( \frac{\partial \zeta}{\partial x} \right)^2 + \left( \frac{\partial \zeta}{\partial y} \right)^2 + \gamma^2 \right) \right) p, \quad (41)$$

with  $\Delta_{x,y} f = \nabla_{x,y} \cdot (\nabla_{x,y} f)$  and  $\zeta$  defined by (12). Therefore, the operator  $\Delta_{sw}^{\gamma}$  can be written under the form of a Sturm-Liouville operator.

## 3.2 Space discretization

Concerning the space discretization, each step – prediction step and correction step – is solved with its own scheme. The method relies on a combination between a finite volume scheme for the hyperbolic part (37) and a finite element scheme for the elliptic part (see the correction step in Section 3.1). The idea is to start with a primal mesh which is triangular, then a dual mesh is built by the finite volume cells centered on the vertices.

Let us consider  $\Omega$  the computational domain with boundary  $\Gamma$ , which is assumed to be polygonal. Let  $\mathcal{T}$  be a triangulation of  $\Omega$ . We denote by  $S_h$  the set of the vertices of the mesh

$$S_h = \{s_i = (x_i, y_i) \in \mathcal{T}\}. \quad (42)$$

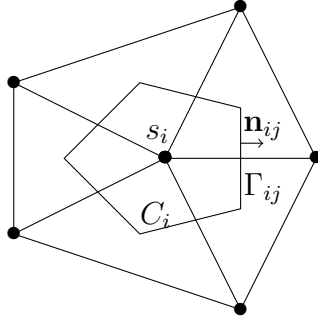


Figure 2: Representation of the dual mesh

We recall here the general formalism of finite volumes on unstructured meshes, and the finite element method we use for the correction part will be detailed in Section 4.

Let us define the finite volume cell  $C_i$  associated to the vertex  $s_i$ . The cells  $C_i$  are built by joining the centers of mass of the triangles surrounding each vertex  $s_i$ . We use the following notations (see Figure 2)

- $|C_i|$ , area of  $C_i$ ,
- $\Gamma_{ij}$ , boundary edge between the cells  $C_i$  and  $C_j$ ,
- $L_{ij}$ , length of  $\Gamma_{ij}$ ,
- $\mathbf{n}_{ij}$ , unit normal to  $\Gamma_{ij}$ , outward to  $C_i$  ( $\mathbf{n}_{ji} = -\mathbf{n}_{ij}$ ),
- $\mathcal{K}_i$  the set of nodes connected to the node  $s_i$ .

**Remark 3.1** *The variables  $H, H\mathbf{u}$  are estimated first as constant mean values on the cells  $C_i$  by the finite volume scheme, which gives the intermediate state  $X^{n+1/2}$ . For the finite element scheme, the state  $X^{n+1}$  is approximated at the vertices of the triangles, and for the required value of  $X^{n+1/2}$  at the node  $s_i$ , we use the constant mean value computed on the cell  $C_i$ . Similarly, for the finite volume step, the required value  $X^{n+1}$  at cell  $C_i$  is given by the value at node  $s_i$ . Therefore, combining the finite volume and the finite element approximations, we will denote by  $X_i$  both the constant mean value on cell  $C_i$  and the value at node  $s_i$ .*

### 3.3 Finite volume scheme for the prediction part

We denote by  $X_i^n$  the approximation of  $X(t^n)$  on a finite volume cell  $C_i$ , the state  $X_i^n$  is the approximation of the cell average of  $X(\mathbf{x}, t^n)$

$$X_i^n \simeq \frac{1}{\text{mes}(C_i)} \int_{C_i} X(\mathbf{x}, t^n) d\mathbf{x}. \quad (43)$$

Then, the approximation of the prediction step (37) can be summarized as follows

$$H_i^{n+1/2} = H_i^n - \sum_{j \in \mathcal{K}_i} \sigma_{ij} \mathcal{F}_H(X_i^n, X_j^n) - \sigma_i \mathcal{F}_H(X_i^n, X_{e,i}^n), \quad (44)$$

$$(\mathbf{H}\mathbf{u})_i^{n+1/2} = (\mathbf{H}\mathbf{u})_i^n - \sum_{j \in \mathcal{K}_i} \sigma_{ij} \mathcal{F}_{H\mathbf{u}}(X_i^n, X_j^n) - \sigma_i \mathcal{F}_{H\mathbf{u}}(X_i^n, X_{e,i}^n), \quad (45)$$

where the quantity  $\sigma_{ij}$  depends on  $\text{mes}(C_i)$ , on  $\Delta t^n$  and on the length of the edges of cells. Similarly,  $\sigma_i = \sigma_{ii}$  is computed for the boundary cells of the domain and  $X_{e,i}^n$  is a fictive state associated to a cell  $C_i$  at the boundary of the domain (see [18]). The numerical fluxes  $\mathcal{F}_H$  (resp.  $\mathcal{F}_{H\mathbf{u}}$ ) are the numerical fluxes corresponding to  $H$  (resp.  $H\mathbf{u}$ ). We do not give details on the flux  $\mathcal{F}$ . For the numerical results presented in this paper, the numerical fluxes are computed by a kinetic solver coupled with a hydrostatic reconstruction technique (see [7]) but other choices are possible. The hydrostatic reconstruction ensures the well-balancing of the scheme (see [7]). In Eq. (45), the boundary conditions (14)-(16) are treated as a Riemann problem at the interface (see [18, 3] for more details about the treatment of the boundary conditions for the shallow water system).

For the third component of Eq. (45), we consider

$$\begin{aligned} (Hw)_i^{n+1/2} = & (Hw)_i^n - \sum_{j \in \mathcal{K}_i} \sigma_{ij} \mathcal{F}_H(X_i^n, X_j^n) \left( w_i^n \mathbf{1}_{\mathcal{F}_H(X_i^n, X_j^n) \geq 0} + w_j^n \mathbf{1}_{\mathcal{F}_H(X_i^n, X_j^n) \leq 0} \right) \\ & - \sigma_i \mathcal{F}_H(X_i^n, X_{e,i}^n) \left( w_i^n \mathbf{1}_{\mathcal{F}_H(X_i^n, X_{e,i}^n) \geq 0} + w_{e,i}^n \mathbf{1}_{\mathcal{F}_H(X_i^n, X_{e,i}^n) \leq 0} \right). \end{aligned} \quad (46)$$

Classically,  $\Delta t^n$  satisfies a CFL condition ensuring the stability of the scheme (mainly domain invariant). Since the resolution of the correction step is implicit, it does not add any constraint over  $\Delta t^n$ .

### 3.4 The mixed problem

Considering now  $X^{n+1/2}$  is given by Eq. (37), we study the mixed problem corresponding to the correction step, that is to say the system (38)-(39), and we give a variational formulation of the problem together with an appropriate treatment of the boundary conditions at the continuous level in order to be compatible with the hyperbolic part. This will make it possible to construct the finite element scheme for this problem. To do so, we consider the domain  $\Omega$  depicted over Fig. 1 with the boundary conditions (14),(16). The correction step consists in computing the shallow water pressure  $p$  in order to satisfy the shallow water divergence free condition (9). Notice that the water depth  $H$  computed by Eq. (44) is not modified by the correction step. Therefore, Eq. (38) reads

$$H^{n+1} = H^{n+1/2}, \quad (47)$$

$$(Hu)^{n+1} + \Delta t^n \left( H^{n+1} \frac{\partial p^{n+1}}{\partial x} + p^{n+1} \frac{\partial \zeta^{n+1}}{\partial x} \right) = (Hu)^{n+1/2}, \quad (48)$$

$$(Hv)^{n+1} + \Delta t^n \left( H^{n+1} \frac{\partial p^{n+1}}{\partial y} + p^{n+1} \frac{\partial \zeta^{n+1}}{\partial y} \right) = (Hv)^{n+1/2}, \quad (49)$$

$$(Hw)^{n+1} - \gamma \Delta t^n p^{n+1} = (Hw)^{n+1/2}, \quad (50)$$

completed with the divergence free condition (39) and the boundary conditions (14),(16). From now on, we drop the superscript  $^{n+1}$  and note  $\Delta t$  for  $\Delta t^n$ , thus the system (48)-(50) and (39) is written

$$H\mathbf{u} + \Delta t \nabla_{sw}^\gamma p = H\mathbf{u}^{n+1/2}, \quad (51)$$

$$\operatorname{div}_{sw}^{\gamma}(\mathbf{u}) = 0, \quad (52)$$

where  $H$  denotes the water depth  $H^{n+1} = H^{n+1/2}$ . This mixed problem in velocity/pressure leads to solving the pressure equation (40), and then to update the velocity with the equation (51). Equations (51)-(52) are the "grad-div" formulation of the problem. The boundary conditions for the system (51)-(52) need to be detailed since they have to be consistent with the prediction part. This is done in the following paragraph.

### 3.4.1 Compatible boundary conditions

In geophysical models such as the shallow water model, it is usual to impose an inflow condition on the inlet  $\Gamma_{in}$ , namely  $H\mathbf{u}$ , and the water depth at the outflow or a free outflow, as defined by (14) and (15). For the hyperbolic step, this choice depends on the Froude number  $Fr = \frac{|\mathbf{u}|}{\sqrt{gH}}$  which characterizes the flow (fluvial or torrential). In this part, we apply compatible boundary conditions on the mixed system depending on the regime chosen for the corresponding Saint-Venant problem at the prediction step. The mixed formulation will allow us to impose boundary conditions on the velocity or the pressure.

**Inflow /outflow** Let us take the two-dimensional inflow  $\mathbf{Q}_e = ((Hu)_e^{n+1/2}, (Hv)_e^{n+1/2})^T$  which is imposed at the hyperbolic part; the vertical velocity  $w_e$  will be treated independently, see Eq. (46). Many strategies can be applied to satisfy compatible boundary conditions. As can be seen in the equations (48)-(49), a natural choice is to keep  $\mathbf{Q}_e$  the same as in the hyperbolic part, then we will impose a condition on the inlet velocity  $\mathbf{u} \cdot \mathbf{n} = (u_e, v_e, w_e)^T \cdot \mathbf{n}$  on  $\Gamma_{in}$ .

Considering the pressure equation (40) and following the procedure detailed in [2], we can deduce that this corresponds to apply a shallow water version of a Neumann boundary condition for the pressure i.e.

$$\nabla_{sw}^{\gamma} p \cdot \mathbf{n} = 0 \text{ on } \Gamma_{in}. \quad (53)$$

In contrast, for the outflow, we impose the water depth in the hyperbolic step and recommend a homogeneous Dirichlet boundary condition for the pressure in order to let the discharge free at the outlet, namely  $p|_{\Gamma_{out}} = p^a = cst$ .

### 3.4.2 Slip boundary conditions

For the wall of the channel represented by  $\Gamma_s$  in Fig. 1, we assume a slip condition for the hyperbolic part  $\mathbf{u}^{n+1/2} \cdot \mathbf{n}|_{\Gamma_s} = 0$  with a Neumann boundary condition for  $H$  (see [18]) and we maintain this condition in the dispersive part, namely  $\mathbf{u} \cdot \mathbf{n}|_{\Gamma_s} = 0$ . Still from the pressure equation (40) and in the same spirit as in [2], we deduce that this leads to having  $\nabla_{sw}^{\gamma} p \cdot \mathbf{n}|_{\Gamma_s} = 0$ . Since  $\frac{\partial H}{\partial x}|_{\Gamma_s} = 0$ , it gives a Neumann-type boundary condition for the pressure  $\frac{\partial p}{\partial \mathbf{n}} = 0$  on  $\Gamma_s$ .

### 3.4.3 The variational formulation

First of all, we assume  $\nabla \zeta \in (L^\infty(\Omega))^2$ ,  $p_0 \in H^{-1/2}(\Gamma)$  and we assume  $H \in L^\infty(\Omega)$  is bounded below and above

$$\alpha_1 < H < \alpha_2, \quad \alpha_1, \alpha_2 > 0. \quad (54)$$

In this section we give the variational formulation of the mixed problem (51)-(52) completed with appropriate boundary conditions

$$\mathbf{u} \cdot \mathbf{n} = \mathbf{u}^{n+1/2} \cdot \mathbf{n} \quad \text{on } \Gamma_{in}, \quad (55)$$

$$\mathbf{u} \cdot \mathbf{n} = 0 \quad \text{on } \Gamma_s, \quad (56)$$

$$p = p_0 \quad \text{on } \Gamma_{out}. \quad (57)$$

In (57), to give a general formulation, we have considered a non-homogeneous Dirichlet boundary condition for the pressure.

Now we distinguish two variational formulations using the shallow water divergence or gradient operator and we explain how to choose the most judicious one in practice. Notice that we switch from one formulation to the other using the relation (13).

**Formulation using the shallow water divergence operator** In this section, we will propose a strong treatment of the boundary condition for the velocity, we introduce the spaces

$$\mathbf{V} = \{ \mathbf{v} \in L^2(\Omega)^3, \operatorname{div}_{sw}^\gamma(\mathbf{u}) \in L^2(\Omega) \}, \quad (58)$$

$$\mathbf{W} = \{ \mathbf{w} \in \mathbf{V}, \mathbf{w} \cdot \mathbf{n} = 0 \text{ on } \Gamma_{in} \cup \Gamma_s \}. \quad (59)$$

The Hilbert space  $\mathbf{W}$  is equipped with inner product  $(\cdot, \cdot)_{\mathbf{W}}$  and induced norm  $\|\cdot\|_{\mathbf{W}} = \|\cdot\|_{(L^2(\Omega))^3} + \|\operatorname{div}_{sw}^\gamma(\cdot)\|_{L^2(\Omega)}$ . For this variational formulation, we assume a homogeneous boundary condition for the velocity, namely, in (55) we take  $\mathbf{u} \cdot \mathbf{n} = 0$  on  $\Gamma_{in}$ .

Then the problem (51)-(52) reads

Find  $\mathbf{u} \in \mathbf{W}$ ,  $p \in L^2(\Omega)$  such that,  $\forall \mathbf{v} \in \mathbf{W}$

$$\int_{\Omega} H \mathbf{u} \mathbf{v} \, d\mathbf{x} - \Delta t \int_{\Omega} \operatorname{div}_{sw}^\gamma(\mathbf{v}) p \, d\mathbf{x} = \int_{\Omega} H \mathbf{u}^{n+1/2} \cdot \mathbf{v} \, d\mathbf{x} - \langle H \mathbf{v} \cdot \mathbf{n}, p_0 \rangle_{\Gamma_{out}}, \quad (60)$$

$$\int_{\Omega} \operatorname{div}_{sw}^\gamma(\mathbf{u}) q \, d\mathbf{x} = 0, \quad \forall q \in L^2(\Omega), \quad (61)$$

where we assume  $p_0 \in H^{-1/2}(\Gamma_{out})$  and  $\langle \cdot, \cdot \rangle_{\Gamma_{out}}$  represents the duality between  $H^{-1/2}(\Gamma_{out})$  and  $H^{1/2}(\Gamma_{out})$  and  $\mathbf{u}^{n+1/2} \in \mathbf{W}$ . We introduce the bilinear forms

$$a(\mathbf{u}, \mathbf{v}) = \int_{\Omega} H \mathbf{u} \cdot \mathbf{v} \, d\mathbf{x}, \quad \forall \mathbf{u}, \mathbf{v} \in \mathbf{V}, \quad (62)$$

$$b_\gamma(\mathbf{v}, q) = - \int_{\Omega} \operatorname{div}_{sw}^\gamma(\mathbf{v}) q \, d\mathbf{x}, \quad \forall \mathbf{v} \in \mathbf{W}, \forall q \in L^2(\Omega). \quad (63)$$

The problem reads

Find  $\mathbf{u} \in \mathbf{W}$ ,  $p \in L^2(\Omega)$  such that

$$a(\mathbf{u}, \mathbf{v}) - \Delta t b_\gamma(\mathbf{v}, p) = a(H \mathbf{u}^{n+1/2}, \mathbf{v}) - \langle H \mathbf{v} \cdot \mathbf{n}, p_0 \rangle_{\Gamma_{out}}, \quad \forall \mathbf{v} \in \mathbf{W}, \quad (64)$$

$$b_\gamma(\mathbf{u}, q) = 0, \quad \forall q \in L^2(\Omega). \quad (65)$$

To impose a non-homogeneous boundary condition on  $\Gamma_s$  for the velocity  $\mathbf{u}$ , we choose  $\mathbf{u} - \bar{\mathbf{u}}_0 \in \mathbf{W}$  where  $\bar{\mathbf{u}}_0$  is defined on  $\bar{\Omega}$  such that  $\bar{\mathbf{u}}_0|_{\Gamma_s} = \bar{\mathbf{u}}^{n+1/2}|_{\Gamma_s}$ .

In practice, this formulation requires to choose basis functions satisfying the slip condition in (59). Therefore, if we want to have a domain with a specific boundary, we will prefer the formulation using the shallow water gradient operator, which is described in the following.



**Formulation using the shallow water gradient operator** We define the spaces

$$Q = \{q \in L^2(\Omega), \nabla_{sw}^\gamma q \in L^2(\Omega)^3\}, \quad (66)$$

$$Q_0 = \{q \in Q, q|_{\Gamma_{out}} = 0\}. \quad (67)$$

Using the duality relation (13), we have

$$\int_{\Omega} \nabla_{sw}^\gamma(q) \cdot \mathbf{u} \, d\mathbf{x} - \int_{\Gamma} q H \mathbf{u} \cdot \mathbf{n} \, ds = 0, \quad \forall q \in Q,$$

then writing

$$\int_{\Gamma} q H \mathbf{u} \cdot \mathbf{n} \, ds = \int_{\Gamma_{in}} q H \mathbf{u} \cdot \mathbf{n} \, ds + \int_{\Gamma_s} q H \mathbf{u} \cdot \mathbf{n} \, ds + \int_{\Gamma_{out}} q H \mathbf{u} \cdot \mathbf{n} \, ds, \quad (68)$$

and, using the boundary conditions (55)-(57), we have

$$\int_{\Gamma} q H \mathbf{u} \cdot \mathbf{n} \, ds = \int_{\Gamma_{in}} q H \mathbf{u}^{n+1/2} \cdot \mathbf{n} \, ds, \quad (69)$$

where the slip boundary condition is imposed in the following weak form  $\int_{\Gamma_s} q H \mathbf{u} \cdot \mathbf{n} = 0, \forall q \in Q$ . We apply the procedure proposed for the Navier-Stokes equations in [37] and we assume there exists  $\bar{p}_0 \in Q$  a given pressure such that  $p_0 = \bar{p}_0|_{\Gamma_{out}} \in H^{1/2}(\Gamma_{out})$ . Therefore, the problem (51)-(52) completed with (55)-(57) reads

Find  $\tilde{p} = p - \bar{p}_0 \in Q_0, p \in Q, \mathbf{u} \in (L^2(\Omega))^3$  such that,

$$\int_{\Omega} (H \mathbf{u} + \Delta t \nabla_{sw} \tilde{p}) \cdot \mathbf{v} \, d\mathbf{x} = \int_{\Omega} H \mathbf{u}^{n+1/2} \cdot \mathbf{v} \, d\mathbf{x}, \quad \forall \mathbf{v} \in (L^2(\Omega))^3, \quad (70)$$

$$\int_{\Omega} \nabla_{sw}^\gamma(q) \cdot \mathbf{u} \, d\mathbf{x} = \int_{\Gamma_{in}} q H \mathbf{u}^{n+1/2} \cdot \mathbf{n} \, ds, \quad \forall q \in Q_0. \quad (71)$$

Finally, we consider the following problem

Find  $\mathbf{u} \in (L^2(\Omega))^3, p \in Q$  such that,  $\forall \mathbf{v} \in (L^2(\Omega))^3$ ,

$$\int_{\Omega} (H \mathbf{u} + \Delta t \nabla_{sw} p) \cdot \mathbf{v} \, d\mathbf{x} = \int_{\Omega} H \mathbf{u}^{n+1/2} \cdot \mathbf{v} \, d\mathbf{x} - \Delta t \int_{\Omega} \nabla_{sw} \bar{p}_0 \cdot \mathbf{v} \, d\mathbf{x}, \quad (72)$$

$$\int_{\Omega} \nabla_{sw}^\gamma(q) \cdot \mathbf{u} \, d\mathbf{x} = \int_{\Gamma_{in}} q H \mathbf{u}^{n+1/2} \cdot \mathbf{n} \, ds, \quad \forall q \in Q_0. \quad (73)$$

As already mentioned, notice that we can use this formulation with the shallow water gradient operator instead of divergence in order to avoid choosing basis functions satisfying the slip boundary condition.

**The pressure equation** Following the procedure of the one-dimensional problem in [2], we set  $\mathbf{v} = \frac{\nabla_{sw}^\gamma(q)}{H}$  in (72) and take homogeneous boundary conditions for the pressure on  $\Gamma$ , it leads to a variational formulation of the problem in the form

$$(\Delta_{sw}^\gamma p, q) = \frac{1}{\Delta t^n} (\operatorname{div}_{sw}^\gamma(\mathbf{u}^{n+1/2}), q), \quad \forall q \in Q_{0,sw}, \quad (74)$$

where

$$Q_{sw} = \{q \in Q, \operatorname{div}_{sw}^\gamma \left( \frac{\nabla_{sw}^\gamma q}{H} \right) \in L^2(\Omega)\},$$

$$Q_{0,sw} = \{q \in Q_{sw}, q|_{\Gamma} = 0\},$$

and the operator  $\Delta_{sw}^\gamma$  is the Laplacian operator defined by (40).

### 3.4.4 The inf-sup condition

We want to establish the inf-sup condition at the continuous level to ensure the problem is well-posed. The so-called inf-sup condition was introduced by Ladyzhenskaya, Babuska and Brezzi in [8, 17, 38] to ensure the well-posedness of mixed problems for incompressible flows and has been studied for the finite element method for instance in [27]. We consider the variational problem with Dirichlet boundary conditions for the pressure (57). The problem (64)-(65) is under the form

Find  $\mathbf{u} \in \mathbf{W}$ ,  $p \in L^2(\Omega)$  such that

$$a(\mathbf{u}, \mathbf{v}) - \Delta t b_\gamma(\mathbf{v}, p) = a(\mathbf{f}, \mathbf{v}) - \langle H\mathbf{v} \cdot \mathbf{n}, p_0 \rangle_{\Gamma_{out}}, \quad \forall \mathbf{v} \in \mathbf{W}, \quad (75)$$

$$b_\gamma(\mathbf{u}, q) = 0, \quad \forall q \in L^2(\Omega), \quad (76)$$

where  $\mathbf{f} \in \mathbf{W}$  is a given vector. For all  $\mathbf{v} \in \mathbf{W}_0 = \{\mathbf{v} \in \mathbf{W}, \operatorname{div}_{sw}^\gamma(\mathbf{v}) = 0\}$ , the problem becomes

Find  $\mathbf{u} \in \mathbf{W}_0$  such that

$$a(\mathbf{u}, \mathbf{v}) = a(\mathbf{f}, \mathbf{v}) - \langle H\mathbf{v} \cdot \mathbf{n}, p_0 \rangle_{\Gamma_{out}}, \quad \forall \mathbf{v} \in \mathbf{W}_0. \quad (77)$$

Under the assumption (54), it is obvious that the bilinear form  $a$  is coercive, i.e. for all  $\mathbf{v} \in \mathbf{W}_0$

$$a(\mathbf{v}, \mathbf{v}) \geq \alpha_1 \|\mathbf{v}\|_{L^2(\Omega)}^2, \quad \alpha_1 > 0. \quad (78)$$

In addition,  $b_\gamma$  is bilinear. With the assumption (54), and  $q \in L^2(\Omega)$  given, if we choose

$$\mathbf{v} = (0, 0, q)^T, \quad (79)$$

then

$$\frac{b_\gamma(\mathbf{v}, q)}{\|q\|_{L^2(\Omega)}} = \gamma \|q\|_{L^2(\Omega)}. \quad (80)$$

This implies the existence and uniqueness of the solution of (60)-(61). For the formulation with the operator  $\nabla_{sw}^\gamma$ , we can use a similar argument and take  $\mathbf{v} = \nabla_{sw}^\gamma(q)$ .

## 4 Finite element approximations for the mixed problem

In this part, we apply a finite element approximation for the correction part (51)-(52), which is suitable to solve the elliptic problem for the pressure. We need two discrete spaces, one for the velocity and one for the approximation of the pressure.

**Sketch of a possible choice.** In practice, the choice of the formulation should be done in function of the boundary conditions. We can summarize the idea by the following

- Unless for very specific cases, it is usual to impose a homogeneous boundary condition for the pressure since we don't know the value of the pressure in real geophysical situations, then the formulations using the gradient or the divergence shallow water operator are both appropriate.

- The choice will also concern the boundary conditions for the velocity, and more precisely for  $\mathbf{u} \cdot \mathbf{n}$ . Using the shallow water divergence operator, it is necessary to build a discrete space with basis functions satisfying slip boundary conditions. In addition, if a discharge is imposed, a lifting of the boundary condition should be applied.
- Besides, we look for a couple of spaces such that the inf-sup condition is satisfied.

In the numerical method presented below, we use the divergence shallow water formulation (see paragraph 3.4.3), with two examples of implementation such that the inf-sup condition is satisfied. Indeed for this formulation, it is straightforward to find spaces such that this condition is verified. Using the same argument as for the continuous problem, we choose spaces such that the conditions (79) and (80) are verified at the discrete level.

The two proposed implementations are, first the  $P_1/P_1$  spaces and then the  $P_1$ -iso $P_2/P_1$  spaces. As usual,  $P_k$  denotes the space of polynomials of two variables of degree  $\leq k$ , and  $P_j/P_i$  denotes the pair of approximation spaces where  $P_j$  is related to the velocity and  $P_i$  is related to the pressure. For the pair  $P_1/P_1$ , the velocity  $w$  is approximated in the same approximation space than the pressure, and for the pair  $P_1$ -iso $P_2/P_1$ , the approximation space of  $w$  contains the approximation space of the pressure (see paragraph 4.2). For both, we give the discrete formulation and we provide a comparison of the numerical results (see Section 6.1) in order to choose the most accurate solution. Since, in this paper, we intend to present simple cases, we will treat numerical applications on domains (rectangles) where the condition  $\mathbf{u} \cdot \mathbf{n} = 0$  reduces to  $u = 0$  or  $v = 0$  (otherwise see [37]).

It is possible to define other function spaces satisfying the inf-sup condition but we have singled out strategies where reduced stencils arise especially due to the difficulties coming from the numerical treatment of the boundary conditions.

## 4.1 The $P_1/P_1$ approximation

For this first implementation, we choose a  $P_1/P_1$  finite element approximation (see [48, 27]) on the primal mesh  $\mathcal{T}$  introduced in paragraph 3.2, on which we approximate the variables at the nodes of the triangles (see Fig. 2). We give the discrete problem with the following boundary conditions

$$p = 0, \text{ on } \Gamma_{out}, \quad (81)$$

$$\mathbf{u} \cdot \mathbf{n} = 0, \text{ on } \Gamma_s \cup \Gamma_{in}. \quad (82)$$

Let us introduce the discrete spaces of approximation:

$$\begin{aligned} V_h &= \{v_h \in C_0(\Omega_h), v_h|_T \in P_1, \forall T \in \mathcal{T}\}, \\ Q_h &= \{q_h \in C_0(\Omega_h), q_h|_T \in P_1, \forall T \in \mathcal{T}\}, \end{aligned}$$

with the dimensions  $\dim(Q_h) = M$ ,  $\dim(V_h) = N$ . We denote  $\mathbf{V}_h = (V_h)^3$ . We use a strong treatment of the boundary condition for the velocity. Therefore, we take

$$\mathbf{u}_h \in \mathbf{W}_h = \{\mathbf{v}_h \in \mathbf{V}_h, \mathbf{v}_h \cdot \mathbf{n}|_{\Gamma_s} = 0\},$$

and  $p_h \in Q_h$  the piecewise linear approximations of  $\mathbf{u}$ ,  $p$  on the triangles of  $\mathcal{T}$ . Notice that the normal components are evaluated by mean for each boundary nodes in order to impose

the slip boundary conditions  $\mathbf{v}_h \cdot \mathbf{n}|_{\Gamma_s} = 0$ . In addition, we assume  $H_h \in V_h$ ,  $\zeta_h \in V_h$ , so we introduce

$$p_h(\mathbf{x}) = \sum_{j \in \mathcal{J}_M} p_j \varphi_j(\mathbf{x}), \quad H_h(\mathbf{x}) = \sum_{i \in \mathcal{I}_N} H_i \varphi_i(\mathbf{x}), \quad (83)$$

$$(H\mathbf{u})_h(\mathbf{x}) = \sum_{i \in \mathcal{I}_N} (H\mathbf{u})_i \varphi_i(\mathbf{x}), \quad \zeta_h(\mathbf{x}) = \sum_{i \in \mathcal{I}_N} \zeta_i \varphi_i, \quad (84)$$

where  $\mathcal{I}_N$  (resp.  $\mathcal{J}_M$ ) is the set of indices of the space  $V_h$  (resp.  $Q_h$ ) and  $\{\varphi_j\}_{j \in \mathcal{J}_M}$  (resp.  $\{\varphi_i\}_{i \in \mathcal{I}_N}$ ) are the basis functions of  $Q_h$  (resp.  $V_h$ ) and

$$\mathbf{u}_h(\mathbf{x}) = \sum_{i \in \mathcal{I}_N} \mathbf{u}_i \varphi_i(\mathbf{x}), \quad (85)$$

with

$$\mathbf{u}_i = \begin{pmatrix} u_i \\ v_i \\ w_i \end{pmatrix} = \frac{1}{H_i} \begin{pmatrix} (Hu)_i \\ (Hv)_i \\ (Hw)_i \end{pmatrix}. \quad (86)$$

**Remark 4.1** Notice that the differences between the two set of indices  $\mathcal{I}_N$  and  $\mathcal{J}_M$  is due to the type of boundary conditions prescribed to the nodes.

We use the definitions (86) in accordance with the finite volume approximation (44)-(45) (see Remark 3.1) and we will use mass lumping in the integrals to be consistent with these definitions.

The discrete formulation of problem (60)-(61) reads

Find  $\mathbf{u}_h \in \mathbf{W}_h$ ,  $p_h \in Q_h$  such that

$$\int_{\Omega} H_h \mathbf{u}_h \cdot \mathbf{v}_h \, d\mathbf{x} + \Delta t \int_{\Omega} \operatorname{div}_{sw}^{\gamma}(\mathbf{v}_h) p_h \, d\mathbf{x} = \int_{\Omega} H_h \mathbf{u}_h^{n+1/2} \cdot \mathbf{v}_h \, d\mathbf{x}, \quad \forall \mathbf{v}_h \in \mathbf{W}_h, \quad (87)$$

$$\int_{\Omega} \operatorname{div}_{sw}^{\gamma}(\mathbf{u}_h) q_h \, d\mathbf{x} = 0 \quad \forall q_h \in Q_h. \quad (88)$$

In order to describe the method, we introduce the following notations

- $S_h = \{s_i = (x_i, y_i) \in \mathcal{T}\}$ : the vertices of the triangular mesh (see (42)),
- $K_{h,i} = \{T \in \mathcal{T} | s_i \in T\}$ : the triangles connected to a vertex  $s_i$ .

Using the definitions (83)-(86), Eq. (87)-(88) become

$$\begin{aligned} & \sum_{i \in \mathcal{I}_N} \left( \int_{\Omega} H_i \mathbf{u}_i \varphi_i(\mathbf{x}) \cdot \mathbf{v}_h(\mathbf{x}) \, d\mathbf{x} \right) - \sum_{j \in \mathcal{J}_M} \Delta t \left( \int_{\Omega} \operatorname{div}_{sw}^{\gamma}(\mathbf{v}_h(\mathbf{x})) \varphi_j(\mathbf{x}) \, d\mathbf{x} \right) p_j \\ & = \sum_{i \in \mathcal{I}_N} \left( \int_{\Omega} H_i \mathbf{u}_i^{n+1/2} \varphi_i(\mathbf{x}) \cdot \mathbf{v}_h(\mathbf{x}) \, d\mathbf{x} \right), \quad \forall \mathbf{v}_h \in \mathbf{W}_h, \end{aligned} \quad (89)$$

completed with the divergence free condition

$$- \sum_{i \in \mathcal{I}_N} \left( \int_{\Omega} \operatorname{div}_{sw}^{\gamma}(\varphi_i) q_h \mathbf{u}_i \, d\mathbf{x} \right) = 0, \quad \forall q_h \in Q_h. \quad (90)$$

We introduce the pressure vector  $P = (p_j)_{1 \leq j \leq M}$  and the velocity vector  $U = (U_1, U_2, U_3)^T$ , with  $U_1 = (u_i)_{1 \leq i \leq N}$ ,  $U_2 = (v_i)_{1 \leq i \leq N}$ , and  $U_3 = (w_i)_{1 \leq i \leq N}$ . Then the problem (89)-(90) can be written as

$$A_H U + \Delta t B_\gamma^T P = A_H U^{n+1/2}, \quad (91)$$

$$B_\gamma U = 0, \quad (92)$$

with the classical notations (see [48]) for the mass matrix  $A_H$ , the divergence operator matrix  $B_\gamma$ . The matrix  $A_H$  depends on the water depth  $H$  and is composed of the three diagonal matrices  $M_H$

$$A_H = \begin{pmatrix} M_H & 0 & 0 \\ 0 & M_H & 0 \\ 0 & 0 & M_H \end{pmatrix},$$

with  $M_{Hji}$  the approximation of  $\sum_{T \in K_{h,i}} \int_T H_i \varphi_i \varphi_j d\mathbf{x}$ . More precisely, using mass lumping we obtain

$$M_{Hji} = \sum_{T \in K_{h,i}} \frac{\text{mes}(T)}{3} H_i \delta_{ij}. \quad (93)$$

We have denoted by  $B_\gamma$  the shallow water divergence operator defined by (90) with  $B_\gamma = (B_{\gamma,1}, B_{\gamma,2}, B_{\gamma,3})$  and using the definition of  $\text{div}_{sw}^\gamma$  in (11), we obtain

$$\begin{aligned} B_{\gamma,1ji} &= - \sum_{T \in K_{h,i}} \int_T \frac{\partial H_h \varphi_i}{\partial x} \varphi_j d\mathbf{x} + \sum_{T \in K_{h,i}} \int_T \varphi_i \varphi_j \frac{\partial \zeta_h}{\partial x} d\mathbf{x}, \\ B_{\gamma,2ji} &= - \sum_{T \in K_{h,i}} \int_T \frac{\partial H_h \varphi_i}{\partial y} \varphi_j d\mathbf{x} + \sum_{T \in K_{h,i}} \int_T \varphi_i \varphi_j \frac{\partial \zeta_h}{\partial y} d\mathbf{x}, \\ B_{\gamma,3ji} &= -\gamma \sum_{T \in K_{h,i}} \int_T \varphi_i \varphi_j d\mathbf{x}. \end{aligned}$$

Finally, the linear system (91)-(92) reads

$$\begin{aligned} \begin{pmatrix} \frac{1}{\Delta t} M_H & 0 & 0 & B_{\gamma,1} \\ 0 & \frac{1}{\Delta t} M_H & 0 & B_{\gamma,2} \\ 0 & 0 & \frac{1}{\Delta t} M_H & B_{\gamma,3} \\ B_{\gamma,1}^T & B_{\gamma,2}^T & B_{\gamma,3}^T & 0 \end{pmatrix} \begin{pmatrix} U_1 \\ U_2 \\ U_3 \\ P \end{pmatrix} \\ = \begin{pmatrix} \frac{1}{\Delta t} M_H & 0 & 0 \\ 0 & \frac{1}{\Delta t} M_H & 0 \\ 0 & 0 & \frac{1}{\Delta t} M_H \\ 0 & 0 & 0 \end{pmatrix} \begin{pmatrix} U_1^{n+1/2} \\ U_2^{n+1/2} \\ U_3^{n+1/2} \end{pmatrix}. \end{aligned} \quad (94)$$

By analogy with the continuous problem, applying the matrix  $B_\gamma$  to the equation (91), we obtain the discrete elliptic equation for the pressure

$$B_\gamma A_H^{-1} B_\gamma^T P = B_\gamma U^{n+1/2}, \quad (95)$$

which is the discretization of the pressure equation (74). We now give some numerical approximations of the integrals we use for each matrix. The matrix  $B$  is computed with the following formulas

$$\begin{aligned}
B_{\gamma,1ji} &= - \sum_{T \in K_{h,i}} \frac{\partial H_h}{\partial x} \Big|_T \int_T \varphi_i \varphi_j \, d\mathbf{x} - \sum_{T \in K_{h,i}} \frac{\partial \varphi_i}{\partial x} \Big|_T \int_T H_h \varphi_j \, d\mathbf{x} \\
&\quad + \sum_{T \in K_{h,i}} \frac{\partial \zeta_h}{\partial x} \Big|_T \int_T \varphi_i \varphi_j \, d\mathbf{x}, \\
B_{\gamma,2ji} &= - \sum_{T \in K_{h,i}} \frac{\partial H_h}{\partial y} \Big|_T \int_T \varphi_i \varphi_j \, d\mathbf{x} - \sum_{T \in K_{h,i}} \frac{\partial \varphi_i}{\partial y} \Big|_T \int_T H_h \varphi_j \, d\mathbf{x} \\
&\quad + \sum_{T \in K_{h,i}} \frac{\partial \zeta_h}{\partial y} \Big|_T \int_T \varphi_i \varphi_j \, d\mathbf{x}, \\
B_{\gamma,3ji} &= -\gamma \sum_{T \in K_{h,i}} \frac{\text{mes}(T)}{3} \delta_{ij}.
\end{aligned}$$

In the first terms of  $B_{\gamma,1ji}$  and  $B_{\gamma,2ji}$ , we use definition (83) of  $H_h$  with mass lumping, and we obtain the following formula

$$\int_T H_h \varphi_j \, d\mathbf{x} = \sum_k \int_T H_k \varphi_k \varphi_j \, d\mathbf{x} = \int_T H_i \varphi_j \, d\mathbf{x} = \frac{\text{mes}(T)}{3} H_i. \quad (96)$$

The projection of the shallow water divergence on a vertex of the mesh is defined by  $\forall \varphi_i \in \mathbf{W}_h, \varphi_j \in Q_h$

$$\text{div}_{sw}^\gamma(\mathbf{u}_h)|_j = \frac{3}{\text{supp}(\varphi_j)} \sum_{i \in \mathcal{I}_N} \int_\Omega \text{div}_{sw}^\gamma(\varphi_i(\mathbf{x})) \varphi_j(\mathbf{x}) \, d\mathbf{x} \, \mathbf{u}_i, \quad (97)$$

where  $\text{supp}(\varphi_j)$  is the area of the support of the function  $\varphi_j$  and is computed by  $\text{supp}(\varphi_j) = \sum_{T \in K_{h,j}} \text{mes}(T)$ .

**Remark 4.2** Notice that mass lumping is chosen for the approximation of  $M_H$  in order to be consistent at the update step

$$A_H U + \Delta t B_\gamma^T P = A_H U^{n+1/2},$$

since  $U^{n+1/2}$  is not written in the same approximation space in the finite volume part, it is more convenient to have a diagonal matrix in practice.

## 4.2 A $\mathbf{P}_1$ -iso $\mathbf{P}_2/\mathbf{P}_1$ approximation

In this part, we propose another approximation by finite elements, using the spaces  $\mathbf{P}_1$ -iso $\mathbf{P}_2/\mathbf{P}_1$  (see [48]) in which we define a coarse triangular mesh  $\mathcal{T}_{2h}$  and a fine mesh  $\mathcal{T}_h$ . The fine mesh corresponds to the primal mesh introduced for the finite volume method 3.3. Unlike the previous approach, the velocity and the pressure are defined in two different spaces. This allows us to approximate the pressure on a coarser mesh than the velocity. Let us introduce the discrete spaces of approximation

$$V_h = \{v_h \in C_0(\Omega_h), \mathbf{v}_h|_\tau \in \mathbf{P}_1, \forall \tau \in \mathcal{T}_h\},$$

$$Q_h = \{q_h \in C_0(\Omega_h), q_h|_T \in P_1, \forall T \in \mathcal{T}_{2h}\},$$

with the dimensions  $\dim(V_h) = N$  and  $\dim(Q_h) = M$ . In addition, we assume  $H_h \in V_h$ . In practice, the triangulation  $\mathcal{T}_h$  is obtained by subdividing each triangle  $T \in \mathcal{T}_{2h}$  into four triangles  $\tau$  by joining the middle of the edges, as shown in Fig. 3.

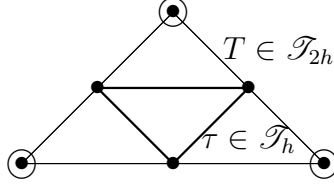


Figure 3: Representation of the triangulation. The velocity is evaluated on the black nodes, while the pressure is evaluated on the circles.

In these spaces of approximation, the velocity is evaluated with the same degrees of freedom as for the  $P_2$  space on the coarse mesh.

In order to describe the method, we introduce the following notations

- $S_h = \{s_i = (x_i, y_i) \in \mathcal{T}_h\}$ : the vertices of the fine mesh,
- $S_{2h} = \{s_j = (x_j, y_j) \in \mathcal{T}_{2h}\}$ : the vertices of the coarse mesh,
- $K_{h,i} = \{\tau \in \mathcal{T}_h | s_i \in \tau\}$ : the triangles of the fine mesh connected to node  $s_i$ ,
- $K_{2h,j} = \{T \in \mathcal{T}_{2h} | s_j \in T\}$ : the triangles of the coarse mesh connected to node  $s_j$ .

We take  $\mathbf{u}_h \in \mathbf{W}_h$  and  $p_h \in Q_h$ , with  $\mathbf{W}_h = \{\mathbf{v}_h \in \mathbf{V}_h, \mathbf{v}_h \cdot \mathbf{n}|_{\Gamma_s} = 0\}$ ,

$$p_h(\mathbf{x}) = \sum_{j \in \mathcal{I}_M} p_j \phi_j(\mathbf{x}), \quad H_h = \sum_{i \in \mathcal{I}_N} H_i \varphi_i(\mathbf{x}), \quad (H\mathbf{u})_h = \sum_{i \in \mathcal{I}_N} (H\mathbf{u})_i \varphi_i(\mathbf{x}),$$

where  $\phi_j$  (resp.  $\varphi_i$ ) are the basis functions of  $Q_h$  (resp.  $V_h$ ) and

$$\mathbf{u}_h(\mathbf{x}) = \sum_{i \in \mathcal{I}_N} \mathbf{u}_i \varphi_i(\mathbf{x}),$$

with  $\mathbf{u}_i$  defined as in (85). Then the matrix  $B$  is computed with the following formulas

$$\begin{aligned} B_{\gamma,1ji} &= - \sum_{T \in K_{2h,i}} \left. \frac{\partial \phi_j}{\partial x} \right|_T \sum_{\tau \in T} \int_{\tau} H_h \varphi_i \, d\mathbf{x} - \sum_{T \in K_{2h,i}} \left. \frac{\partial H_h}{\partial x} \right|_T \sum_{\tau \in T} \int_{\tau} \phi_j \varphi_i \, d\mathbf{x} \\ &\quad + \sum_{T \in K_{2h,i}} \sum_{\tau \in T} \left. \frac{\partial \zeta_h}{\partial x} \right|_{\tau} \int_{\tau} \varphi_i \phi_j \, d\mathbf{x}, \\ B_{\gamma,2ji} &= - \sum_{T \in K_{2h,i}} \left. \frac{\partial \phi_j}{\partial y} \right|_T \sum_{\tau \in T} \int_{\tau} H_h \varphi_i \, d\mathbf{x} - \sum_{T \in K_{2h,i}} \left. \frac{\partial H_h}{\partial y} \right|_T \sum_{\tau \in T} \int_{\tau} \phi_j \varphi_i \, d\mathbf{x} \\ &\quad + \sum_{T \in K_{2h,i}} \sum_{\tau \in T} \left. \frac{\partial \zeta_h}{\partial y} \right|_{\tau} \int_{\tau} \varphi_i \phi_j \, d\mathbf{x}, \end{aligned}$$

$$B_{\gamma,3ji} = -\gamma \sum_{T \in K_{2h,i}} \sum_{\tau \in T} \int_{\tau} \varphi_i \phi_j d\mathbf{x}.$$

As for (96), we choose  $H_h$  and  $z_{bh}$  linear on each triangle  $\tau \in \mathcal{T}_h$  and we use mass lumping

$$\int_{\tau} H_h \varphi_i d\mathbf{x} = H_i \frac{\text{mes}(\tau)}{3},$$

and

$$\int_{\tau} \varphi_i \phi_j d\mathbf{x} = \frac{\text{mes}(\tau)}{3} \sum_{\mathbf{x} \in \bar{s}(\tau)} \varphi_i(\mathbf{x}) \phi_j(\mathbf{x}),$$

where  $s(\tau) = \{v_0, v_1, v_2\}$  are the three vertices of the triangle  $\tau$ . Finally, the discrete version of the shallow water divergence operator is defined for each vertex of the coarse mesh by  $\forall \varphi_i \in \mathbf{W}_h, \phi_j \in Q_h$

$$\text{div}_{sw}^{\gamma}(\mathbf{u}_h)|_j = \frac{3}{\text{supp}(\phi_j)} \sum_{i \in \mathcal{I}_N} \int_{\Omega} \text{div}_{sw}^{\gamma}(\varphi_i(\mathbf{x})) \phi_j(\mathbf{x}) d\mathbf{x} \mathbf{u}_i. \quad (98)$$

This definition is used numerically and can be seen as a diagonal preconditioner to solve Eq. (95).

## 5 Numerical algorithm

In this section, we give details about the procedure we use to combine the finite volume method and the finite element method. For the sake of clarity, we just give an overview of the steps of the algorithm. Assuming we know  $H^n, H\mathbf{u}^n$ , the combined finite volume/finite element method (37)-(39) can be summarized by the following steps

- Solve the hyperbolic part (37) with the finite volume scheme (44)-(45) and get  $(H, H\mathbf{u})^{n+1/2}$ . Because of Eq. (47), we obtain  $H^{n+1}$  as well.
- Solve the elliptic problem (95) to obtain  $p^{n+1}$ . We use the iterative method described below.
- Update the velocity  $\mathbf{u}^{n+1}$  in the correction step (91) using  $\nabla_{sw}^{\gamma} p^{n+1}$ .

### 5.1 Iterative methods

The linear problem (91)-(92) leading to (95), is solved in practice with iterative methods. Several algorithms allow us to solve the classical mixed problem (51)-(52) in the divergence form. This is usually applied to the finite element method for the Navier-Stokes equations, see [48, 37]. We describe here the Conjugate Gradient method (CG) and the Uzawa algorithm (see [41, 48]) which use the duality property of the operators. In practice, to take the boundary conditions into account, the matrix consists in two blocks in which one part contains the elements of  $B_{\gamma} A_H^{-1} B_{\gamma}^T$  for all the nodes that have to be solved and another diagonal part which is the identity and corresponds to impose Dirichlet conditions for the pressure. Then



the contribution of the matrix  $B_\gamma$  associated with the given pressure is affected on the right hand side. The linear problem can be written

$$\begin{pmatrix} \mathcal{A} & 0 \\ 0 & Id \end{pmatrix} P = \begin{pmatrix} \frac{1}{\Delta t} \mathcal{D} - \mathcal{A}_G P_G \\ P_G \end{pmatrix}, \quad (99)$$

where  $\mathcal{A}$  is the matrix extracted from  $B_\gamma A_H^{-1} B_\gamma^T$  corresponding to the fact that we restrict to the nodes of unknowns, respectively  $\mathcal{A}_G$  to the nodes of the given pressure  $P_G$ . The matrix  $\mathcal{D}$  is the shallow water divergence vector of the velocity at the unknown nodes at the prediction part. This reduces the size of the problem and allows us to apply the Conjugate Gradient algorithm. The initialization is done with the state  $(Hu, Hv, Hw)^{n+1/2}$  computed at the hyperbolic step. For the sake of clarity, we drop the superscripts  $n+1/2$  and we denote with the superscript  $(k)$  the index iteration of the iterative method. In addition, we use the notation  $f = \frac{1}{\Delta t} \mathcal{D} - \mathcal{A}_G P_G$ . Then the CG algorithm can be summarized as

Initialization

$$\begin{aligned} U^{(0)}, P^{(0)} & \text{ given,} \\ r^{(0)} & = f - \mathcal{A}P^{(0)}, \\ d^{(0)} & = r^{(0)}. \end{aligned}$$

For  $k > 0$

$$\begin{aligned} \rho & = \frac{(r^{(k)}, d^{(k)})}{(d^{(k)}, \mathcal{A}d^{(k)})}, \\ P^{(k+1)} & = P^{(k)} + \rho d^{(k)}, \\ r^{(k+1)} & = r^{(k)} - \rho \mathcal{A}d^{(k)}, \\ \delta^{(k+1)} & = \frac{\|r^{(k+1)}\|^2}{\|r^{(k)}\|^2}, \\ d^{(k+1)} & = r^{(k+1)} + \delta^{(k+1)} d^{(k)}. \end{aligned}$$

Then, the correction is applied to the velocity.

For the description of the Uzawa method, let us now use the duality between the operators (40) and (11), keeping the notations

$$\begin{aligned} U^{(0)}, P^{(0)} & \text{ given,} \\ P^{(k+1)} & = P^{(k)} + \alpha B_\gamma U^{(k)}, \\ A_H U^{(k+1)} & = A_H U^{n+1/2} - \Delta t B_\gamma^T P^{(k+1)}, \end{aligned}$$

with  $\alpha$  chosen such that  $0 < \alpha < \frac{2}{\max \lambda_i}$  with  $\lambda_i$  the eigenvalues of  $B_\gamma A_H^{-1} B_\gamma^T$ . The CG algorithm adapted for problem (91)-(92) in the form of the Uzawa algorithm reads

Initialization

$$\begin{aligned} U^0 & = U^{n+1/2}, \\ d^{(0)} & = r^{(0)} = B_\gamma U^{(0)}, \end{aligned}$$

$k > 0$

$$\alpha^{(k)} = \frac{(r^{(k)}, d^{(k)})}{(B_\gamma^T d^{(k)}, A_H^{-1} B_\gamma^T d^{(k)})},$$

$$\begin{aligned} P^{(k+1)} &= P^{(k)} + \alpha^{(k)} d^{(k)}, \\ Z &= A_H U^{n+1/2} - \Delta t B_\gamma^T P^{(k+1)}. \end{aligned}$$

Solve the system  $A_H U^{(k+1)} = Z$  (we recall that the matrix  $A_H$  is diagonal since we have used mass lumping).

Compute  $B_\gamma U$

$$\begin{aligned} r^{(k+1)} &= B_\gamma U^{(k+1)}, \\ \delta^{(k+1)} &= \frac{\|r^{(k+1)}\|^2}{\|r^{(k)}\|^2}, \\ d^{(k+1)} &= r^{(k+1)} + \delta^{(k+1)} d^{(k)}. \end{aligned}$$

In accordance with Eqs. (97),(98), the norm  $\|\cdot\|$  used in the above iterative algorithms takes into account the normalization of the operators by the basis function support area.

## 5.2 Wet-dry interface

As one can see, the method presented above requires the water depth does not vanish since the resolution of the equation for the pressure (40) requires dividing the shallow water gradient by  $H$ . At the discrete level, this difficulty arises in the mass matrix (93). But in practice, it is necessary the model be able to capture dry/wet interfaces e.g. when considering wave propagation over obstacles like islands or reaching a coast line.

In practice, we introduce a small parameter  $\varepsilon$  such that the pressure equation (40) returns  $p = 0$  when  $H$  tends to zero. This can be viewed as a Dirichlet condition on the dry zone of the domain, such that the pressure equation is solved only on the wet domain. In the iterative solver, this leads to testing the value of the water depth for each node  $s_j$  of the mesh (or for the coarse mesh if the P<sub>1</sub>-isoP<sub>2</sub>/P<sub>1</sub> approximation is used). However, in order to avoid selecting a list of dry nodes at each time step, which would require significant computation time, we solve the whole problem and we introduce a threshold

$$\varepsilon \ll 1, \tag{100}$$

under which the water depth is redefined by  $\varepsilon$ , namely  $H_\varepsilon = \max(H, \varepsilon)$ . Since the mass matrix  $M_H$  is weighted with  $H$  and needs to be inverted in the correction step, to avoid having singularities, the matrix is redefined with respect to  $H_\varepsilon$  as

$$M_{H_\varepsilon ji} = \sum_{T \in K_{h,i}} \int_T H_\varepsilon \varphi_i \varphi_j d\mathbf{x}.$$

Then, at the correction step, the shallow water gradient is redefined by

$$\nabla_{sw}^{\gamma, \varepsilon} p|_i = \frac{\mathbb{1}_{H_i > H_\varepsilon}}{\text{supp}(\varphi_i)} \sum_j \int_\Omega \nabla_{sw}^\gamma (\varphi_j) \cdot \varphi_i d\mathbf{x} p_j, \tag{101}$$

so the velocity is not updated at these nodes by step (38). In Eq. (101), the function  $\varphi_j$  is replaced by  $\phi_j$  if we use P<sub>1</sub>-isoP<sub>2</sub>/P<sub>1</sub> space approximation. Notice that introducing  $H_\varepsilon$  does

not change the result since it appears only in the terms of degree zero for the derivative of the pressure. It only prevents from redefining wet/dry zones at each iteration. With these definitions, the Laplacian operator written in (41) becomes

$$\Delta_{sw}^{\gamma,\varepsilon} p = \operatorname{div}_{sw}^{\gamma} \left( \frac{\nabla_{sw}^{\gamma} p}{H_{\varepsilon}} \right) = \nabla_{x,y} \cdot (H \nabla_{x,y} p) + \left( \Delta \zeta - \frac{1}{H_{\varepsilon}} \left( \left( \frac{\partial \zeta}{\partial x} \right)^2 + \left( \frac{\partial \zeta}{\partial y} \right)^2 + \gamma^2 \right) p \right). \quad (102)$$

### 5.3 An improved time scheme

The numerical methods presented in the previous sections can be improved if we apply a Heun scheme, which is based on a Runge-Kutta method, to the Saint-Venant model and the correction part. This improvement has been detailed for the one-dimensional problem in [2] and can be straightforwardly applied to the two-dimensional case. The Heun scheme is slightly modified so that the stability (CFL) condition remains valid. For this system, our scheme is second order accurate in time and, if we use a MUSCL like extension based on limited reconstructed values at interfaces (see [7]) in the hyperbolic step, it is formally second order accurate in space (see [7]). However, with the correction step, the resulting scheme is no longer of order two, but introducing the Heun scheme and the reconstruction in the hyperbolic step can improve the global accuracy of the scheme. This will be illustrated in the next section.

## 6 Numerical validation

In this section, we confront the numerical procedure with several test cases. First, we present convergence curves for two time dependent analytical solutions allowing to validate the numerical resolution. Then comparisons with experimental data and in the situation of an earthquake-generated tsunami are performed enforcing the validity of the model. From some of the analytical and experimental test cases, we investigate the influence of the chosen value for the parameter  $\gamma$ .

### 6.1 A solitary wave

The solitary wave is a one-dimensional non-stationary analytical solution of the model. This solution has been proposed to validate the one-dimensional model in [2] and has the form

$$H = H_0 + a \left( \operatorname{sech} \left( \frac{x - c_0 t}{l} \right) \right)^2,$$

and we deduce

$$\begin{aligned} u &= c_0 \left( 1 - \frac{d}{H} \right), \\ w &= -\frac{c_0 d}{\gamma} \frac{\partial(\ln H)}{\partial x}, \\ p &= -\frac{c_0 d H}{\gamma^2} \left( \frac{\partial^2(\ln H)}{\partial x \partial t} + c_0 \left( 1 - \frac{d}{H} \right) \frac{\partial^2(\ln H)}{\partial x^2} \right), \end{aligned}$$

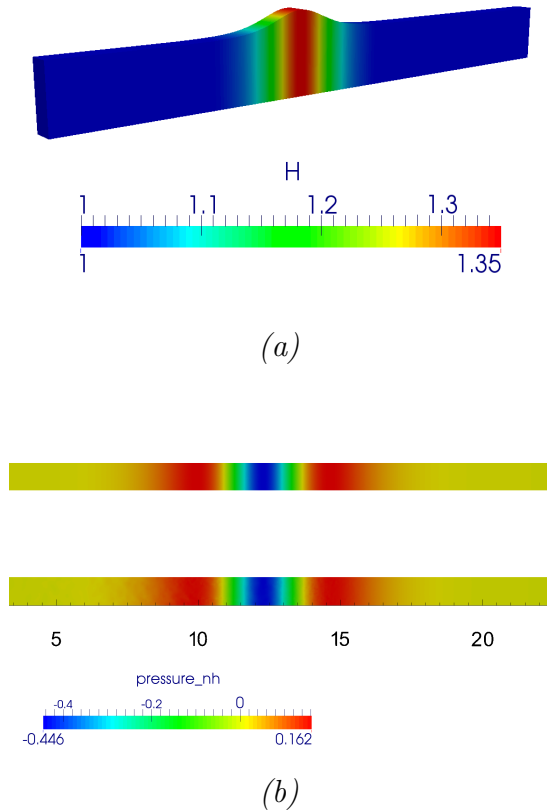


Figure 4: Illustration of the solitary wave propagation at  $t = 1.99$  s, (a) computed water depth (lateral view) and (b) non-hydrostatic pressure (top view), analytical solution at the top, numerical field below.

with  $d, a, H_0 \in \mathbb{R}$ ,  $H_0 > 0$ ,  $a > 0$  and  $c_0 = \frac{H_0}{d} \sqrt{g(H_0 + a)}$ ,  $l = \frac{2H_0}{\gamma} \sqrt{\frac{H_0}{a} + 1}$ .

This analytical solution is extended to two dimensions in a rectangular channel and the definition  $v = 0$  is added to the previous equations.

We consider a channel of dimension 30 m  $\times$  1 m, the water elevation  $H_0$  is set to 1 m with significant wave amplitude  $a = 0.35$  m and  $d = 1$  m. On the model domain in Figure 1a, we set a slip boundary condition for  $\Gamma_s$ , a given discharge for the inlet (14) and a water elevation at the outlet (15) with a homogeneous Dirichlet boundary condition for the pressure at the correction step. The test case is initialized with the analytical solution in the domain and we observe the propagation of the wave over time.

In Fig. 4, we show the computed water depth (Fig. 4-(a)) and the computed and analytical pressures (Fig. 4-(b)). Notice that the numerical results have been obtained for  $\gamma = 2$  but since it is an analytical solution, any other choice for  $\gamma$  would have given the same results. This has been obtained with the  $P_1$ -iso $P_2/P_1$  approximation and the wave has covered approximately one wavelength.

A numerical comparison of the  $P_1/P_1$  and  $P_1$ -iso $P_2/P_1$  approximations is proposed in order to choose the most accurate one for practical applications. In Fig. 5, we compare the numerical solutions, computing the  $P_1/P_1$  solution on the fine mesh of the  $P_1$ -iso $P_2/P_1$ , here

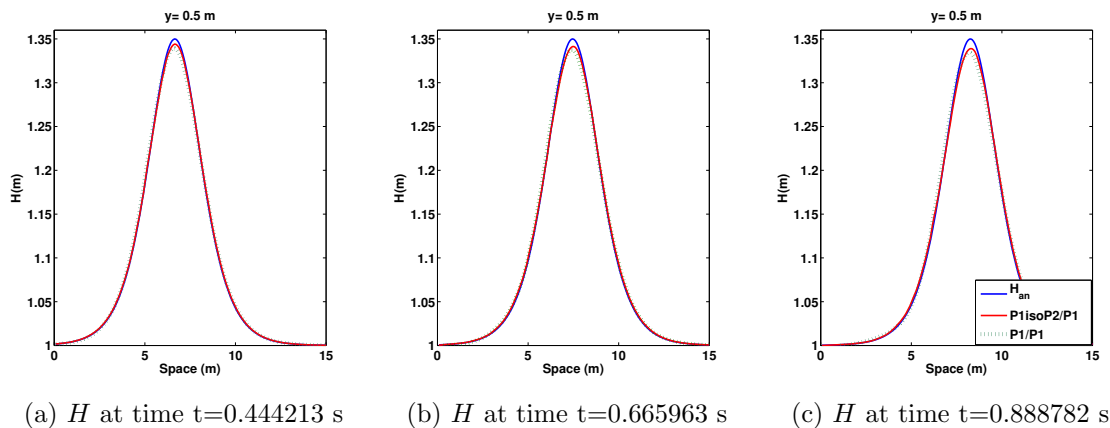


Figure 5: Comparison between the analytical water depth  $H_{an}$  and the  $P_1$ iso $P_2/P_1$  and the  $P_1/P_1$  approximations on the solitary wave propagation.

an unstructured mesh of 72770 nodes. After a short time, the  $P_1/P_1$  method provides a less accurate solution than the  $P_1$ -iso $P_2/P_1$  approximation, since we observe the amplitude of the wave obtained by the  $P_1$ -iso $P_2/P_1$  method is closer to the analytical solution than the  $P_1/P_1$  approximation.

Since the comparison gives better results with the  $P_1$ -iso $P_2/P_1$  spaces, we opt for this approximation to validate the method. We apply the "improved" method presented in paragraph 5.3 and obtain a good approximation of the soliton during all the propagation (see Fig. 6), we observe that the solitary wave conserves its amplitude over the time. The simulation shown in Fig. 6 was computed with 251330 nodes for the fine mesh. We study the convergence rate of the computed solutions, computing the  $L^2$  error at time  $t = 1.99$  s for different meshes of triangle's mean edges  $h_0 = 0.0493528$  m,  $h_1 = 0.0250468$  m and  $h_2 = 0.016781$  m. Figure 7 shows the logarithm of the  $L^2$  error between the analytical solution and the numerical solution with respect to  $\log\left(\frac{h_0}{h}\right)$  where  $h = h_i, i = 0, 1, 2$ . We observe a convergence rate close to 1 for the first order method, while with the improved scheme we still obtain approximately a first order convergence rate, although the computed error is smaller.

Notice that the simulations have also been carried out when, at the initial instant, the soliton is outside of the considered domain. The simulation results and the convergence curve are exactly the same, see [2]. It is a good indicator of the quality of the numerical treatment of the boundary conditions.

## 6.2 A periodic analytical solution with wet-dry interfaces

In this section the objective is to validate the method with a non stationary analytical solution where the free surface oscillates over the time. Such solutions have been introduced by Thacker in [50] for the shallow water equations and can be obtained over a paraboloid topography with a velocity  $(u, v)$  varying only with respect to time. In the following proposition, we extend the result proposed by Thacker to the case of the non-hydrostatic model (7)-(9).

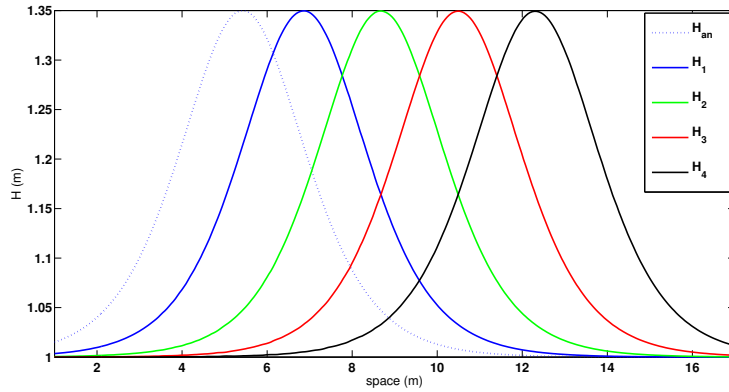


Figure 6: Cross section at the center of the channel  $y = 0.5$  m; water depth of the analytical solution at initial time  $H_0 = H_{an}$  and computed solution  $H(t_i), i = 1, \dots, 4$  with  $t_0 = 0$  s,  $t_1 = 0.499805$  s,  $t_2 = 0.999871$  s,  $t_3 = 1.49983$  s,  $t_4 = 1.99993$  s for the  $P_1$ -iso $P_2/P_1$  approximation and the improved method (Heun scheme).

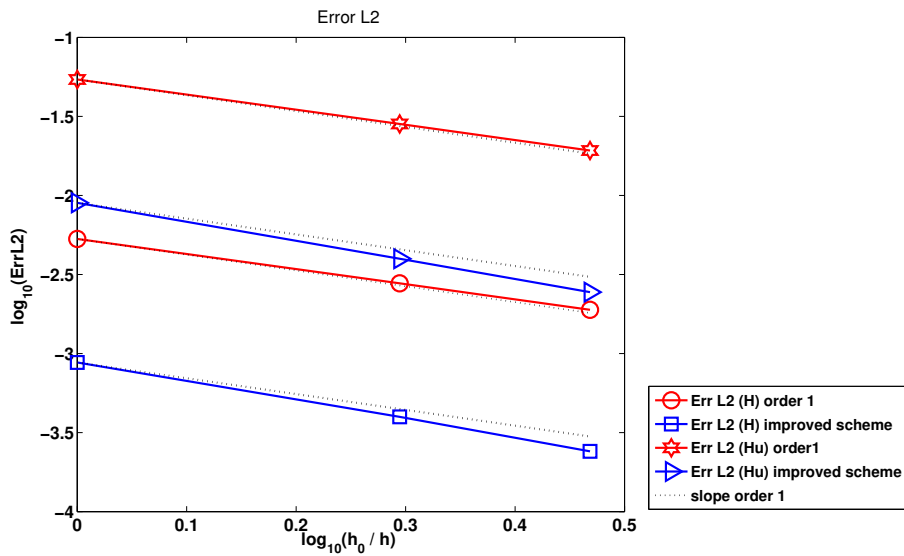


Figure 7: Convergence rate for the  $P_1$ -iso $P_2/P_1$  approximation for the classical scheme (order 1 in time and space) and the improved method (Heun scheme and reconstruction in the prediction step). The  $L^2$  error is computed at time  $t = 1.99$  s

**Proposition 6.1** Let  $H_0 \in \mathbb{R}_+$ ,  $(\alpha, \beta) \in \mathbb{R}^2$  with  $|\alpha\beta| \leq 1$  and

$$\omega^2 = \frac{\alpha g}{1 - \alpha^2 \beta^2}.$$

Then the variables  $H, u, v, w, p, s$  defined by

$$\begin{aligned} H(x, y, t) &= \max\left(0, H_0 - \frac{\alpha}{2}(x - \beta \cos(\omega t))^2 - \frac{\alpha}{2}(y - \beta \sin(\omega t))^2\right), \\ u(x, y, t) &= -\beta\omega \sin(\omega t), \\ v(x, y, t) &= \beta\omega \cos(\omega t), \\ w(x, y, t) &= -\alpha\beta\omega(\sin(\omega t)x - \cos(\omega t)y), \\ p(x, y, t) &= \frac{\beta^2\alpha\omega^2}{2}H, \\ s(x, y, t) &= \alpha\beta\omega^2(\sin(\omega t)x - \cos(\omega t)y), \end{aligned}$$

with the topography

$$z_b(x, y) = \alpha \frac{x^2 + y^2}{2},$$

are solutions of the model

$$\begin{aligned} \frac{\partial H}{\partial t} + \nabla_0 \cdot (H\mathbf{u}) &= 0, \\ \frac{\partial(H\mathbf{u})}{\partial t} + \nabla_0 \cdot (H\mathbf{u} \otimes \mathbf{u}) + \nabla_0 \left(\frac{g}{2}H^2\right) + \nabla_{sw}^\gamma p &= -gH\nabla_0(z_b) + S, \\ \operatorname{div}_{sw}^\gamma(\mathbf{u}) &= 0, \end{aligned}$$

with  $S = (0, s)^T$  corresponding to the model (7)-(9) with  $\gamma = 2$  and completed with the source term  $s$ .

*Proof of prop. 6.1* The proof relies on simple computations and is not detailed here. ■

**Remark 6.1** The proposition 6.1 is valid only for  $\gamma = 2$ , see also [19]. And it is worth noticing that, as proved in [19], the solution proposed in prop. 6.1 is also an analytical solution for the full Euler system (17)-(18),(19)-(21). Thus the model  $\mathcal{M}_\gamma$  for  $\gamma = 2$  shares common analytical solutions with the Euler system, this has already been mentioned in paragraph 2.3.3.

We run this test on a disc domain centered in  $(x, y) = (0, 0)$  with a radius of 5 m, with  $\alpha = 0.3 \text{ m}^{-1}$ ,  $\beta = 1.6 \text{ m}$  and  $H_0 = 1.0 \text{ m}$  as shown in Figure 8. This case is simulated with 440746 nodes for the fine mesh (and 220588 for the coarse mesh). We use the strategy proposed in paragraph 5.2 to treat the wet-dry front with  $\varepsilon$  defined by (100),  $\varepsilon = 10^{-5} \text{ m}$  and we impose a discharge equal to zero at the boundary conditions (14) and a Dirichlet boundary condition for the pressure on  $\Gamma$ . In Fig. 8, the representation of the free surface oscillating in the bowl is shown for different time steps. The Figure 9 presents the profile of the elevation in the cross-section  $y = 0$  at different time steps compared with the analytical solution. This is a crucial test case for the validation of the method since we test the dry/wet - wet/dry transitions and strong variations of the free surface. We also compute the convergence rate with the same formula described for the solitary case (see paragraph 6.1) for different meshes where  $h_0 = 0.0551138 \text{ m}$ ,  $h_1 = 0.0412458 \text{ m}$ ,  $h_2 = 0.0330043 \text{ m}$ ,  $h_3 = 0.0274674 \text{ m}$ ,

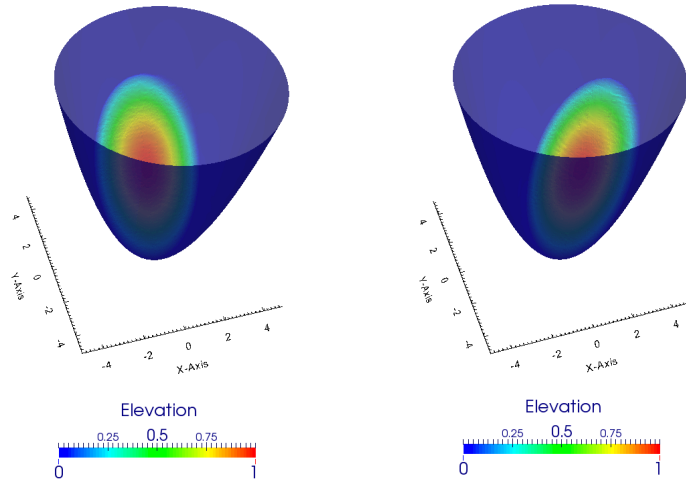


Figure 8: Simulation of the free surface oscillations in a paraboloid at different time steps.

where  $h_i$ ,  $i = 0, \dots, 3$  are the mean edges of the meshes. In Figures 10 and 11 we observe that the convergence rate is close to one for the water depth, the vertical discharge  $Hw$  and the non-hydrostatic pressure  $p$ . These simulated results are computed with the improved method described in 5.3 and as expected, we obtain a similar slope for  $Hw$  and  $p$  and a better convergence for  $H$  which is not corrected in the second step of the scheme (38).

### 6.3 Dingemans experiments - effect of the choice of $\gamma$

The experiments carried out by Dingemans [24] at Delft Hydraulics deal with the wave propagation over uneven bottoms. A small amplitude wave (0.02 m) is generated at the left boundary of a closed basin with vertical shores. At rest, the water depth in the channel varies from 0.4 m to 0.1 m, see Fig. 13. Eight sensors recording the free surface elevation are located at abscissa 2 m, 4 m, 10.5 m, 12.5 m, 13.5 m, 14.5 m, 15.7 m and 17.3 m.

Since the studied model (7)-(9) depends on a parameter  $\gamma$ , we have tried to investigate the impact of the parameter value. The values  $\gamma = 3/2$  – corresponding the Green-Naghdi model – and the value  $\gamma = 2$  – corresponding to the model proposed by some of the authors – have been tested and the simulations results are depicted in Figs. 13.

It appears over Figs. 13 that either for  $\gamma = 2$  or for  $\gamma = 3/2$ , the simulation results are rather in good agreement with the recorded data. Nevertheless, we can see over Figs. 13 that the Green-Naghdi model i.e. when  $\gamma = 3/2$  gives better results than the model for  $\gamma = 2$ . This is in accordance with the fact that the Green-Naghdi model is well adapted for gravity waves propagation whereas for advection dominant flows, the value  $\gamma = 2$  can be singled out, see remark. 6.1.

**Remark 6.2** *As mentioned in Section 2,  $\gamma$  can be any real number with  $\gamma > 1$ . The values  $\gamma = 2$  and  $\gamma = 3/2$  corresponding to existing models are mainly used. It is important to notice that in the case of the Dingemans experiments, with values of  $\gamma$  very different from 2 and 3/2 e.g.  $\gamma = 5$ , the obtained results are worse but not significantly different, See Fig. 14.*



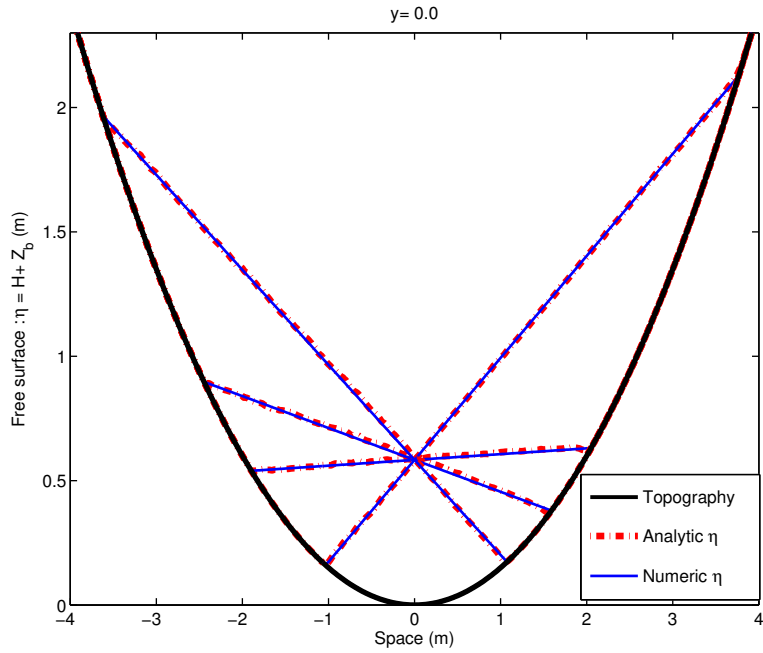


Figure 9: Cross section of the free surface at  $y = 0$  of the free surface  $H + z_b$  compared with the analytical solution at different times:  $t_0 = 0.277222$  s,  $t_1 = 0.431123$  s,  $t_2 = 0.739382$  s,  $t_3 = 0.893419$  s and  $t_4 = 1.20134$  s.

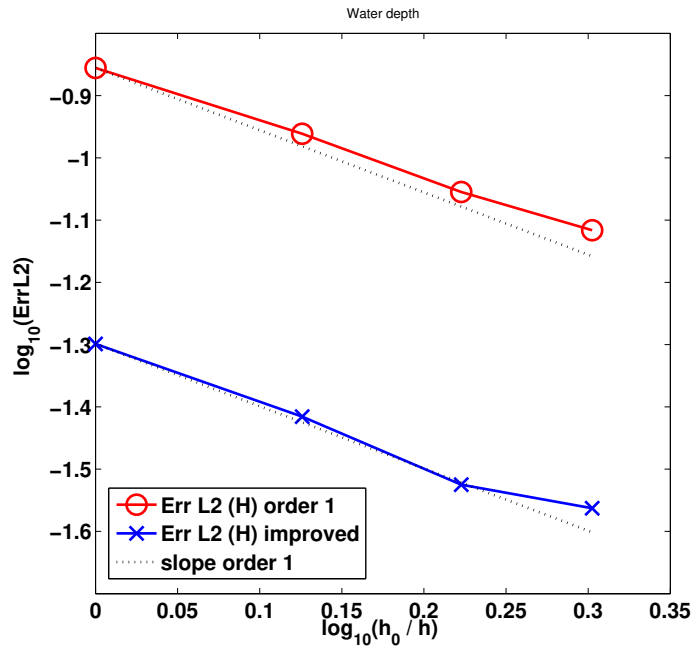


Figure 10: Convergence rate of the  $L^2$  error of the water depth.

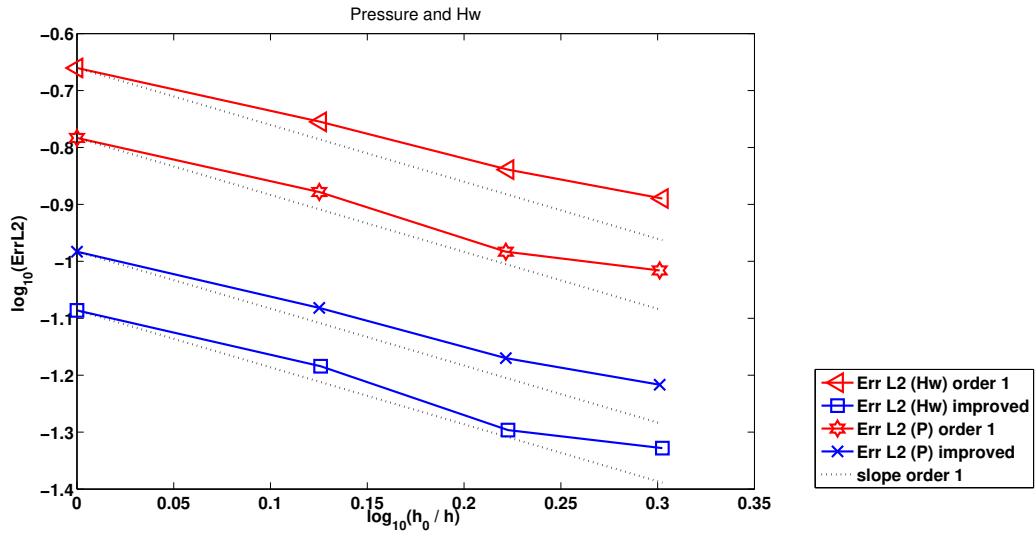


Figure 11: Convergence rate of the vertical discharge and the pressure.

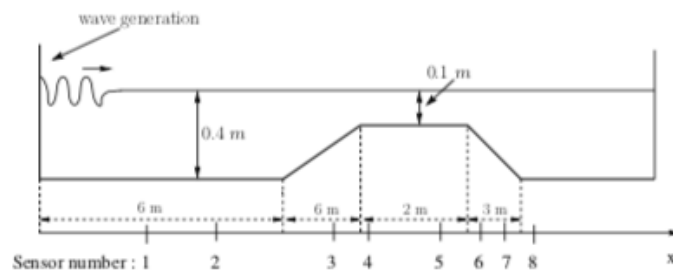


Figure 12: Channel profile for the experiments and location of the sensors.

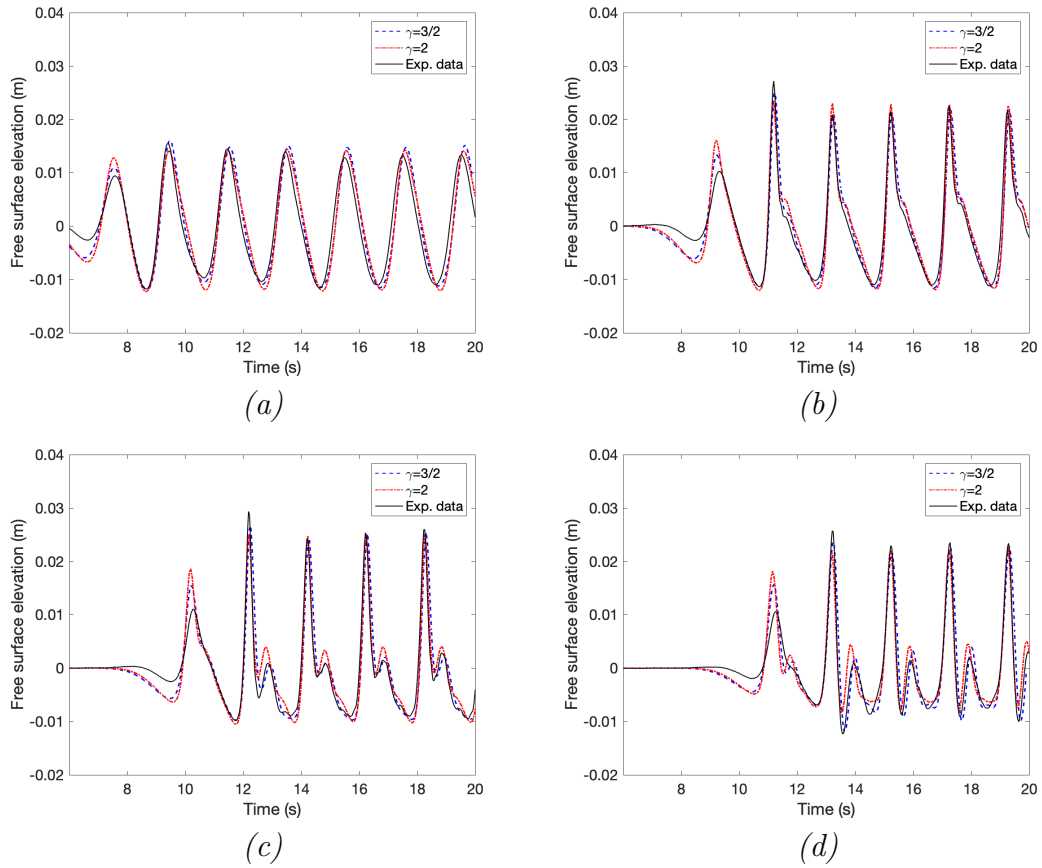


Figure 13: Comparisons between the experimental data (solid line) and the simulations of the dispersive model with  $\gamma = 3/2$  (dashed line) and  $\gamma = 2$  (dashed-dotted line). Figs. (a), (b), (c) and (d) respectively correspond to the results for the sensors 3, 4, 5 and 6.

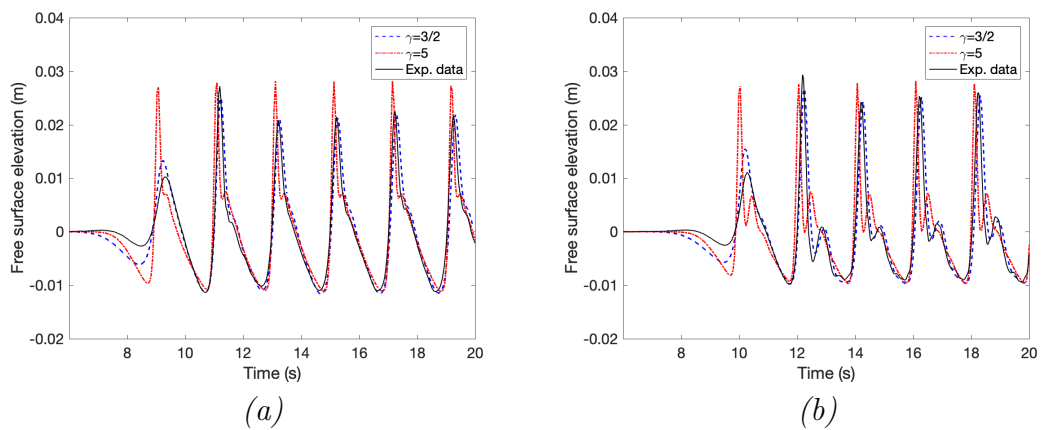


Figure 14: Comparisons between the experimental data (solid line) and the simulations of the dispersive model with  $\gamma = 3/2$  (dashed line) and  $\gamma = 5$  (dashed-dotted line). Figs. (a), (b) respectively correspond to the results for the sensors 4 and 5.

## 6.4 Application to the 2014 Iquique earthquake, Chile

In this section we apply the depth-averaged model (7)-(9) to a real geophysical event, i.e. an earthquake-generated tsunami. On April 1, 2014 at 23:46:47 UTC, a 8.2 magnitude earthquake struck off the coast of northern Chile and generated a tsunami. The earthquake was localized at 95km NW of Iquique (see Figure 15) and the elevation of the water depth was recorded by the Deep-ocean Assessment and Reporting of Tsunamis (DART) buoys of the NOAA center for tsunami research [1]. The objective of this section is to confront the results of the hydrostatic and non-hydrostatic shallow water models to the water wave measurements of the DART buoys. To simulate the tsunami generated earthquake, we use a topography given by the NOAA and two different sources, denoted by Source A and Source B, describing the displacement of the topography during the earthquake (Figure 16a and 16b). The sources A and B have been obtained from different joined inversion of seismic, GPS and tsunami data ([51] and Martin Vallée, personal communication). These sources have been chosen because of their different spatial variability : source A (Fig. 16a) is overall more symmetric and smoother than source B (Fig. 16b). As dispersive effects are expected to be more important for shorter wavelength spatial heterogeneities, we investigate here the relative importance of dispersive effects for these two sources. In particular, we compare the simulations using both the hydrostatic and non-hydrostatic models on two gauges represented in Figure 17a and corresponding to the location of

- the closest DART buoy: DART-32401 localized at 260 NM West-Southwest of Arica, Chile at Latitude/Longitude coordinates (-20.473, -73.429).
- a point denoted S, localized at coordinates (-21.98702, -71.14027), closer to the coast and next to the trench where bathymetry variations are huge.

The simulation is made on a spatial domain covering an area of  $800 \text{ km} \times 1200 \text{ km}$  (Figures 15 and 17). For the initial conditions, we prescribe (i) a horizontal free surface for the water and (ii) the bathymetry before the earthquake occurred (Fig. 17). The topography associated with the unstructured mesh is obtained by a linear interpolation of the ETOPO1 Arc-Minute Global Relief Model [5]. According to the comments in paragraph 2.3.3 and the results obtained in paragraph 6.3, the value  $\gamma = 2$  has been chosen for the simulations. Notice that with  $\gamma = 3/2$ , the simulation results are very similar in the sense that the differences cannot be seen with the naked eye.

The initial instant of the simulation exactly corresponds to the trigger point of the seism. The earthquake is simulated by updating the bathymetry at the first time step. The imposed bottom displacement is illustrated in Figure 16 for sources A and B. For the non-hydrostatic simulation, the fine mesh – on which the velocity is computed – has 470174 nodes which gives a size of edge’s triangle of about 2.5 km, while the coarse mesh - on which the pressure is computed - has 117088 nodes. The hydrostatic simulation has been performed on the fine mesh. We use the improved order accuracy in time and space for both simulations.

Figure 18 shows that non hydrostatic effects generate waves with higher frequencies, as expected. In Figure 19a, we compare the simulated water waves obtained with source A using the hydrostatic and non-hydrostatic models with the waves recorded at the DART buoy 32401. The simulation pretty well reproduces the first wave in terms of amplitude and phase. The higher frequency oscillation of the water surface are not at all captured by the hydrostatic model (dashed line). These oscillations may result from more complex effects like dispersion.

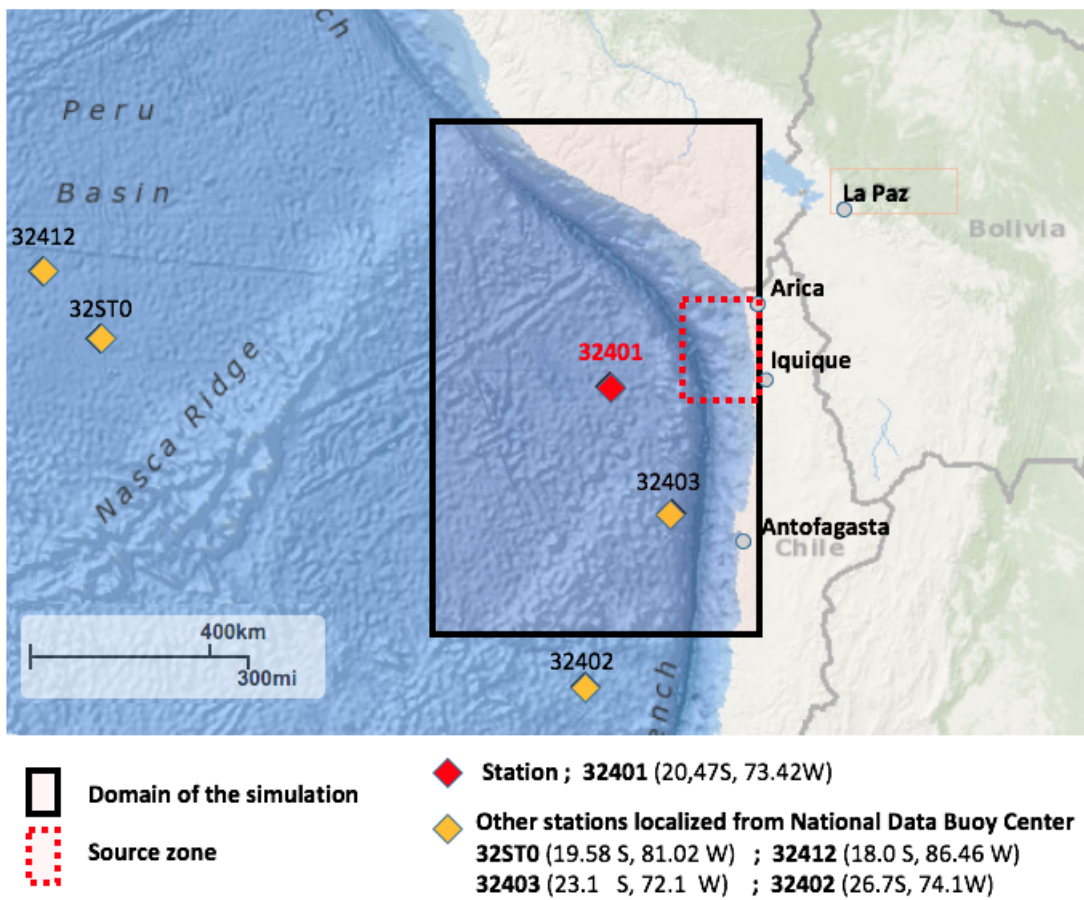


Figure 15: Map of the Chilean coast with localization of the simulated domain. Localization of the DART buoy 32401 and the other reference DART buoys (see NOAA's data).

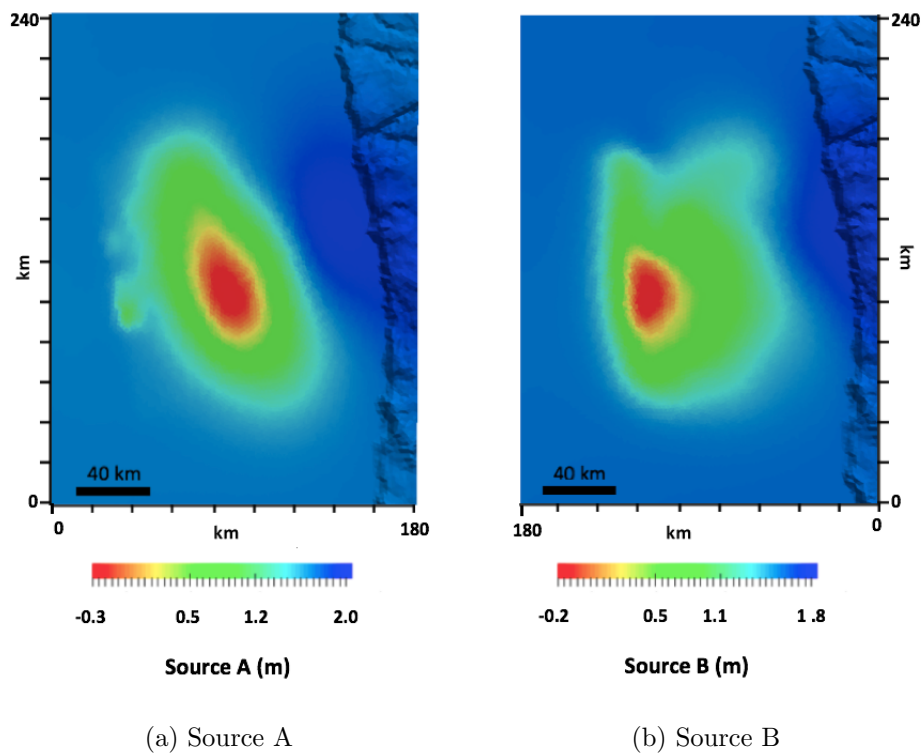
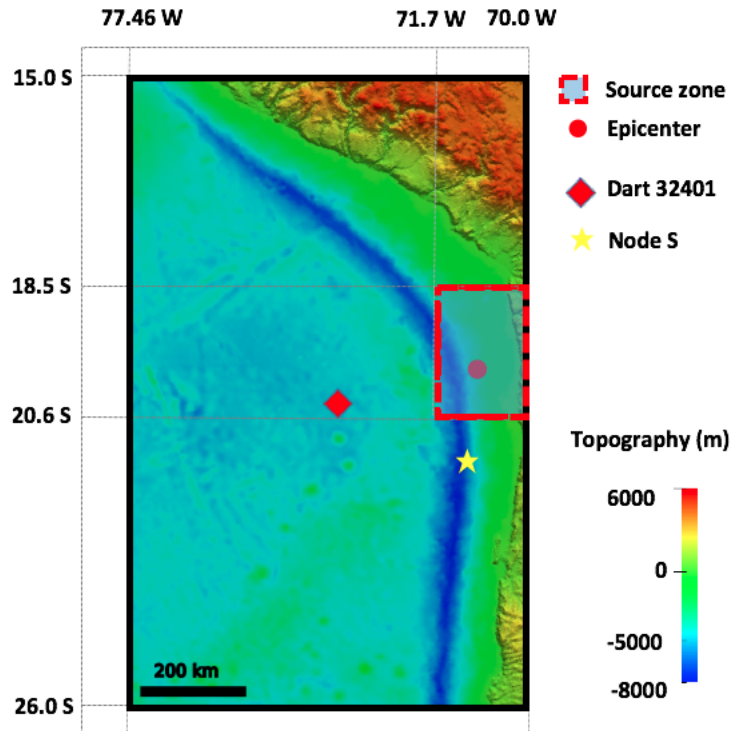
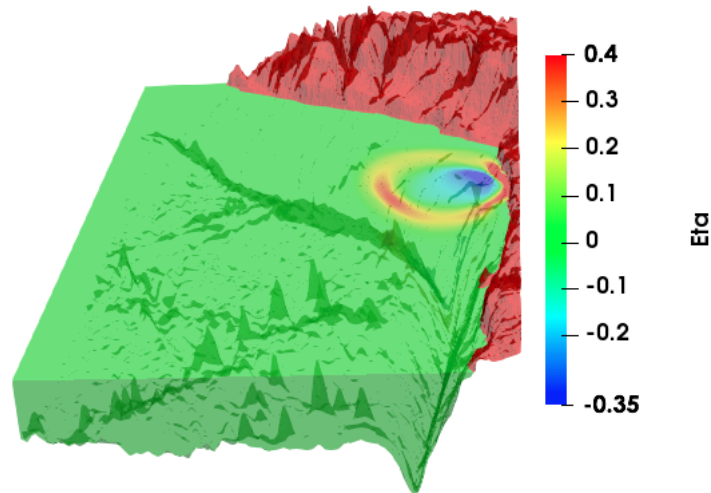


Figure 16: Imposed displacement for (a) source A and (b) source B. The selected zone corresponds to the source zone in red shown in Figure 15.

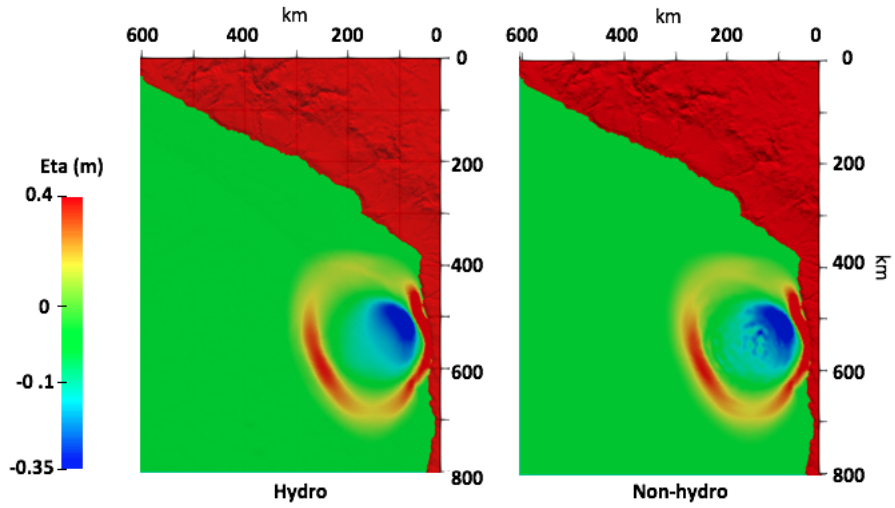


(a) Domain of the simulation: localization of the observed nodes and topography (m)

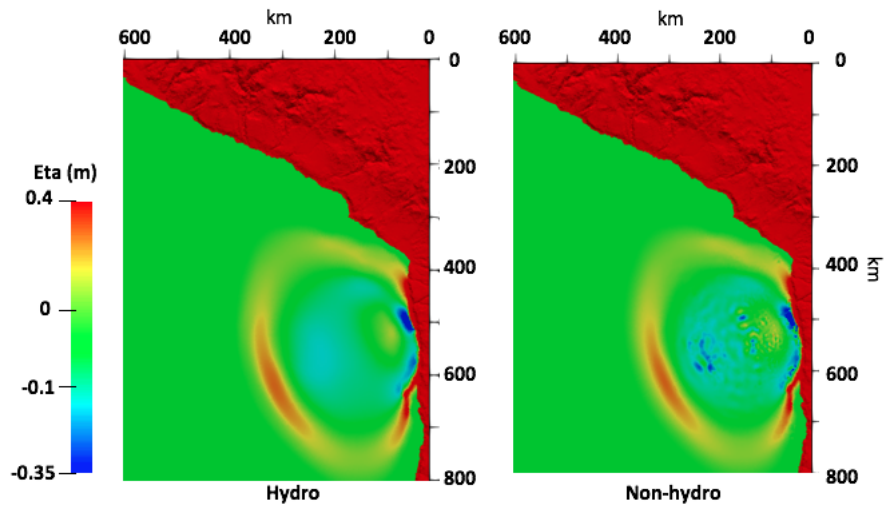


(b) Computational domain at  $t = 666$  s.

Figure 17: (a) Topography and bathymetry of the simulation domain (Chile) and location of the earthquake epicenter, the DART buoy 32401 and the gauge S. (b) Simulated free surface variation  $\eta$  of the tsunami wave at time 666 s.



(a)  $t = 666$  s



(b)  $t = 999$  s

Figure 18: Comparison of the wave front for the hydrostatic (left) and the non-hydrostatic (right) model at time  $t = 666$ s and  $t = 999$  s and using the source A. The coordinate (0,0) corresponds to the coordinate (15.0 S, 70.0 W).



The non-hydrostatic (DAE) model produces indeed higher frequencies than the hydrostatic model. However these higher frequencies oscillations are very small compared to the observed ones. As a result, in this case the dispersion effects do not seem to play a significant role.

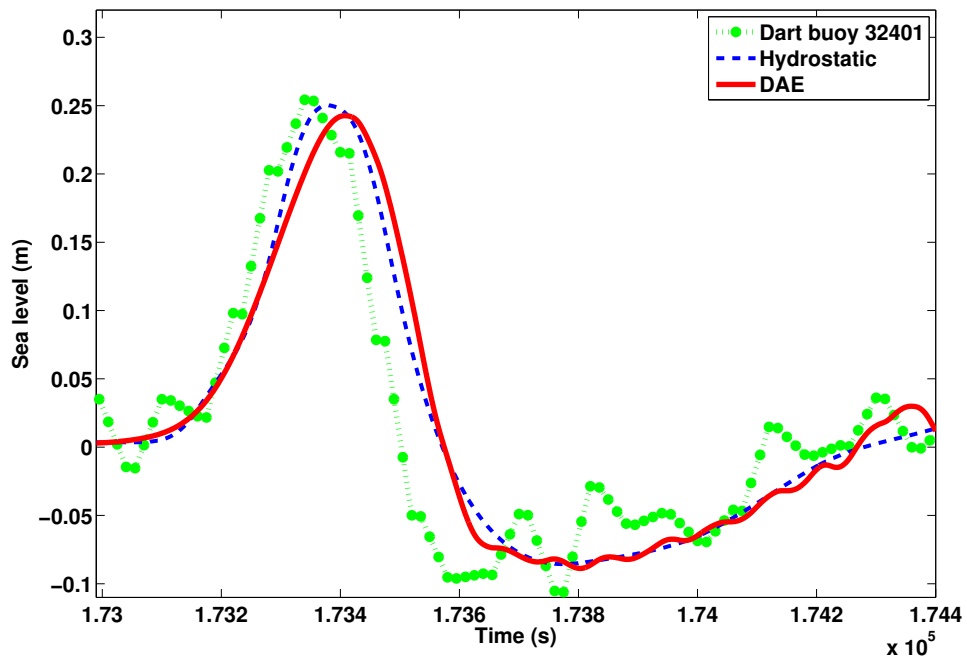
In Figure 19b, we do the same comparison with simulations based on the more heterogeneous source B. Although the simulated maximum amplitude and the phase of the first wave is further from the observation, the differences between the hydrostatic and non-hydrostatic models are larger. In particular, the non-hydrostatic model generates an oscillation at higher frequency (between times around 1.734 s and 1.737 s) followed by smaller fluctuations. This oscillation bare some similarities with the oscillation that follows the first wave in the observations (between times around 1.735 and 1.738 s), even though the phase is different and the amplitude of the negative part is smaller than the recorded wave.

The ability of the DAE model to generate higher frequencies is illustrated on the waves simulated at gauge S for the two sources (Figure 20a). At this location, there are strong gradients of the bathymetry (see Figure 17a), that are expected to enhance non-hydrostatic effects . We observe indeed that at this location, dispersive effects are more important for both sources and produce high frequency oscillations. Interestingly, the two sources give very different high frequency waves, suggesting that detailed comparison between simulation and observation in this frequency range may provide insight into the source heterogeneity, providing non-hydrostatic effects are properly accounted for. Further investigation of the impact of detailed source characteristics on high frequency waves would be very interesting but beyond the scope of this paper. A big issue is the numerical cost of such non-hydrostatic simulations making it difficult to perform sensitivity analysis since a very fine mesh is required to obtained converged numerical solutions.

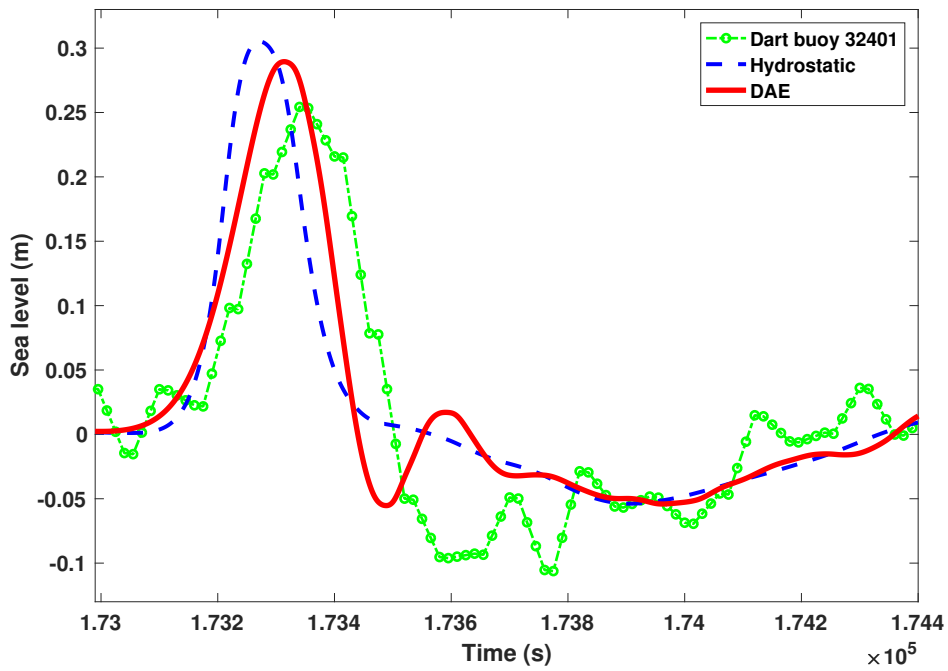
## 7 Conclusion

In this paper, we have presented a new method for a family of two-dimensional dispersive shallow water systems, where we do not solve equations containing high order derivatives but a mixed problem in velocity and pressure. This allows to applying the method with appropriate boundary conditions for the velocity and the pressure, which is usually a difficult task when high order equations are solved. In addition, due to the general framework of the method and the definition of the shallow water operators, i.e. the duality property on which the method is based, the algorithm has been applied on unstructured meshes using a combined finite volume / finite element method to solve a hyperbolic system on the one hand and an elliptic equation on the other hand. The algorithm uses an iterative method of Uzawa type to solve the elliptic problem. We provided a numerical validation with two analytical solutions. We have proved that our model is applicable at the scale of geophysical events by simulating an earthquake generated tsunami in Chili. Our simulations pretty well reproduce the recorded wave. Our results show that, in a real situation, strong differences may be obtained between hydrostatic and non-hydrostatic simulations, depending on the variability of the topography around the recorded gauge and on the source heterogeneity.

Compared to classical finite volume schemes for the approximation of the shallow water equations, the proposed strategy for the resolution of these dispersive models only add the resolution of a linear elliptic-type equation. Nevertheless, the iterative inversion of the elliptic operator significantly increases the computational costs and an optimized technique e.g. using a preconditioning is required. Moreover, the proposed method can be extended to layer-

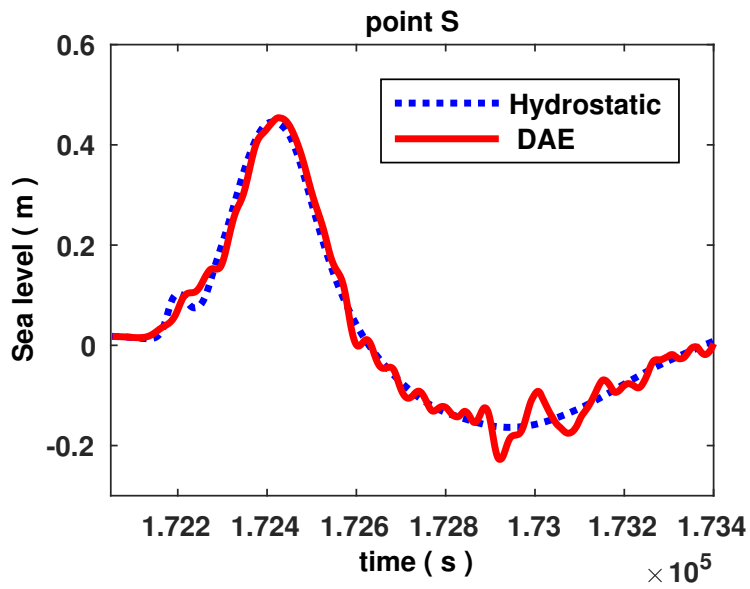


(a) Source A

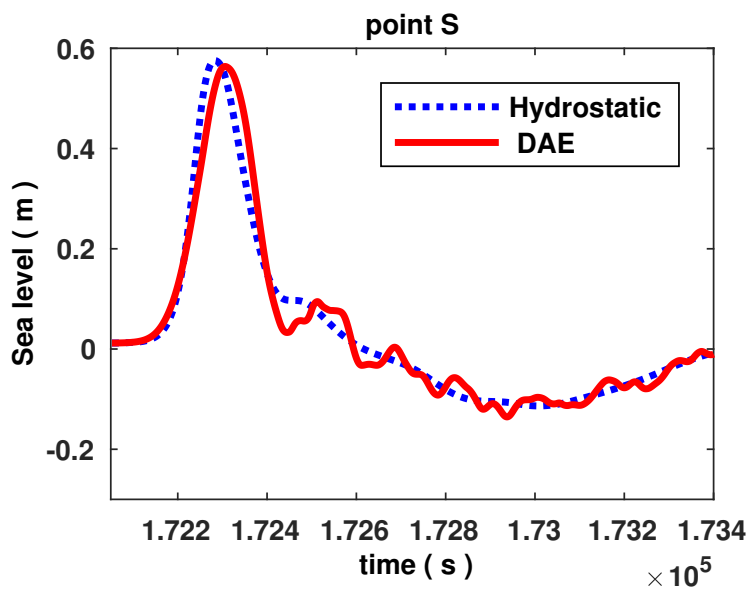


(b) Source B

Figure 19: Comparison between numerical results using both models (hydrostatic and non-hydrostatic) and the data of the DART buoy 32401 for (a) source A and (b) source B.



(a) Source A



(b) Source B

Figure 20: Comparison between numerical results using both models (hydrostatic and non-hydrostatic) at the node S for (a) source A and (b) source B.

averaged approximations of the 3d Euler system [?], this work is in progress.

## Acknowledgments

The authors thank Robert Eymard for his helpful and constructive discussions that greatly contributed to improve the final version of the paper and Martin Vallée, Sebastien Allgeyer and Raphaël Gradin for providing the inverted sources for the tsunami simulation and for fruitful discussions. The authors acknowledge the Inria Project Lab Algae in Silicio for its financial support. The first author received a partial grant from the Fondation Ledoux. This research is also supported by the ANR MIMOSA project and the ERC SLIDEQUAKES ERC-CG-2013-PE10-617472.

## References

- [1] NOAA home page. <https://www.ngdc.noaa.gov/mgg/global/global.html>, 2017.
- [2] N. Aïssiouene, M.-O. Bristeau, E. Godlewski, and J. Sainte-Marie. A combined finite volume - finite element scheme for a dispersive shallow water system. *Networks and Heterogeneous Media*, 11(1):1–27, 2016.
- [3] S. Allgeyer, M.-O. Bristeau, D. Froger, R. Hamouda, A. Mangeney, J. Sainte-Marie, F. Souillé, and M. Vallée. Numerical approximation of the 3d hydrostatic Navier-Stokes system with free surface. working paper or preprint, Sept. 2017.
- [4] B. Alvarez-Samaniego and D. Lannes. Large time existence for 3D water-waves and asymptotics. *Invent. Math.*, 171(3):485–541, 2008.
- [5] C. Amante and B. Eakins. ETOPO1 1 Arc-Minute Global Relief Model: Procedures, Data Sources and Analysis. Research report, National Geophysical Data Center, NOAA, 2009.
- [6] E. Audusse, F. Bouchut, M.-O. Bristeau, R. Klein, and B. Perthame. A fast and stable well-balanced scheme with hydrostatic reconstruction for Shallow Water flows. *SIAM J. Sci. Comput.*, 25(6):2050–2065, 2004.
- [7] E. Audusse and M.-O. Bristeau. A well-balanced positivity preserving second-order scheme for Shallow Water flows on unstructured meshes. *J. Comput. Phys.*, 206(1):311–333, 2005.
- [8] I. Babuska. The finite element method with lagrangian multipliers. *Numerische Mathematik*, 20:179–192, 1972/73.
- [9] A.-J.-C. Barré de Saint-Venant. Théorie du mouvement non permanent des eaux avec applications aux crues des rivières et à l’introduction des marées dans leur lit. *C. R. Acad. Sci. Paris*, 73:147–154, 1871.
- [10] J. Behrens and F. Dias. New computational methods in tsunami science. *Philos Trans A Math Phys Eng Sci.*, Oct 28(373):(2053), 2015.

- [11] J. Bona, M. Chen, and J.-C. Saut. Boussinesq equations and other systems for small-amplitude long waves in nonlinear dispersive media: Part I. Derivation and linear theory. *J. Nonlinear Sci.*, 12:283–318, 2002.
- [12] J.-L. Bona, T.-B. Benjamin, and J.-J. Mahony. Model equations for long waves in nonlinear dispersive systems. *Philos. Trans. Royal Soc. London Series A*, 272:47–78, 1972.
- [13] P. Bonneton, E. Barthélemy, F. Chazel, R. Cienfuegos, D. Lannes, F. Marche, and M. Tissier. Recent advances in Serre-Green Naghdi modelling for wave transformation, breaking and runup processes. *European Journal of Mechanics - B/Fluids*, 30(6):589 – 597, 2011. Special Issue: Nearshore Hydrodynamics.
- [14] P. Bonneton, F. Chazel, D. Lannes, F. Marche, and M. Tissier. A splitting approach for the fully nonlinear and weakly dispersive Green-Naghdi model. *J. Comput. Phys.*, 230(4):1479–1498, Nov. 2010.
- [15] F. Bouchut. *Nonlinear stability of finite volume methods for hyperbolic conservation laws and well-balanced schemes for sources*. Birkhäuser, 2004.
- [16] D. Bresch, E. Fernandez-Nieto, I. Ionescu, and P. Vigneaux. Augmented Lagrangian Method and Compressible Visco-Plastic Flows : Applications to Shallow Dense Avalanches. In *New Directions in Mathematical Fluid Mechanics*, Advances in Mathematical Fluid Mechanics, pages 57–89. Birkhäuser, Jan. 2010.
- [17] F. Brezzi. On the existence, uniqueness and approximation of saddle-point problems arising from Lagrangian multipliers. *Rev. Française Automat. Informat. Recherche Opérationnelle Sér. Rouge*, 8(R-2):129–151, 1974.
- [18] M.-O. Bristeau and B. Coussin. Boundary Conditions for the Shallow Water Equations solved by Kinetic Schemes. Rapport de recherche RR-4282, INRIA, 2001. Projet M3N.
- [19] M.-O. Bristeau, A. Mangeney, J. Sainte-Marie, and N. Seguin. An energy-consistent depth-averaged euler system: Derivation and properties. *Discrete and Continuous Dynamical Systems - Series B*, 20(4):961–988, 2015.
- [20] R. Camassa, D. D. Holm, and C. D. Levermore. Long-time effects of bottom topography in shallow water. *Phys. D*, 98(2-4):258–286, 1996. Nonlinear phenomena in ocean dynamics (Los Alamos, NM, 1995).
- [21] F. Chazel, D. Lannes, and F. Marche. Numerical simulation of strongly nonlinear and dispersive waves using a Green–Naghdi model. *J. Sci. Comput.*, 48(1-3):105–116, July 2011.
- [22] A. J. Chorin. Numerical solution of the Navier-Stokes equations. *Math. Comp.*, 22:745–762, 1968.
- [23] R. Cienfuegos, E. Barthélemy, and P. Bonneton. A fourth-order compact finite volume scheme for fully nonlinear and weakly dispersive Boussinesq-type equations. Part I: Model development and analysis. *Internat. J. Numer. Methods Fluids*, 51(11):1217–1253, 2006.

- [24] M.-W. Dingemans. *Wave propagation over uneven bottoms*. Advanced Series on Ocean Engineering - World Scientific, 1997.
- [25] A. Duran and F. Marche. Discontinuous-Galerkin discretization of a new class of Green-Naghdi equations. *Communications in Computational Physics*, 17(3):721–760, Oct. 2014.
- [26] A. Duran and F. Marche. A discontinuous Galerkin method for a new class of Green-Naghdi equations on simplicial unstructured meshes. *Appl. Math. Model.*, 45:840–864, 2017.
- [27] G. Ern. *Theory and Practice of Finite Elements*. Springer-Verlag New York, 2004.
- [28] C. Escalante, T. Morales, and M.-J. Castro. Weakly dispersive shallow water flows: an efficient implementation using a finite-volume finite-difference scheme. In *Proceedings of the XXIV congress on differential equations and applications XIV congress on applied mathematics*, pages 255–259, Cadiz, 2015.
- [29] E. D. Fernandez-Nieto, M. Parisot, Y. Penel, and J. Sainte-Marie. A hierarchy of dispersive layer-averaged approximations of Euler equations for free surface flows. *Communications in Mathematical Sciences*, 16(5):1169–1202, 2018.
- [30] A. Filippini, M. Kazolea, and M. Ricchiuto. A Flexible 2D Nonlinear Approach for Nonlinear Wave Propagation, Breaking and Run up. In *ISOPE 2017 - Proceedings of the Twenty-seventh International Ocean and Polar Engineering Conference*, San Francisco, CA, United States, June 2017.
- [31] J.-F. Gerbeau and B. Perthame. Derivation of Viscous Saint-Venant System for Laminar Shallow Water; Numerical Validation. *Discrete Contin. Dyn. Syst. Ser. B*, 1(1):89–102, 2001.
- [32] S. Glimsdal, G. K. Pedersen, C. B. Harbitz, and F. Løvholt. Dispersion of tsunamis: does it really matter? *Natural Hazards and Earth System Sciences*, 13(6):1507–1526, 2013.
- [33] E. Godlewski and P.-A. Raviart. *Numerical approximations of hyperbolic systems of conservation laws*. Applied Mathematical Sciences, vol. 118, Springer, New York, 1996.
- [34] A. Green and P. Naghdi. A derivation of equations for wave propagation in water of variable depth. *J. Fluid Mech.*, 78:237–246, 1976.
- [35] J.-L. Guermond. Some implementations of projection methods for Navier-Stokes equations. *ESAIM: Mathematical Modelling and Numerical Analysis*, 30(5):637–667, 1996.
- [36] J.-L. Guermond and J. Shen. On the error estimates for the rotational pressure-correction projection methods. *Math. Comput.*, 73(248):1719–1737, 2004.
- [37] F. Hecht and C. Pares. NSP1B3 : un logiciel pour résoudre les équations de Navier Stokes incompressible 3D. Research Report RR-1449, INRIA, 1991. Projet MENUSIN.
- [38] O. Ladyzhenskaya. *The mathematical theory of viscous incompressible flow*. New York: Gordon and Breach, 1969.

- [39] D. Lannes. *The water waves problem*, volume 188 of *Mathematical Surveys and Monographs*. American Mathematical Society, Providence, RI, 2013. Mathematical analysis and asymptotics.
- [40] D. Lannes and F. Marche. A new class of fully nonlinear and weakly dispersive Green-Naghdi models for efficient 2D simulations. *J. Comput. Phys.*, 282:238–268, 2015.
- [41] P. Lascaux and R. Theodor. *Analyse numérique matricielle appliquée à l’art de l’ingénieur*. Masson, 1986.
- [42] O. Le Métayer, S. Gavriluk, and S. Hank. A numerical scheme for the Green-Naghdi model. *J. Comput. Phys.*, 229(6):2034–2045, 2010.
- [43] R. LeVeque. *Numerical methods for conservation laws*. Birkhauser, 1999.
- [44] P. Lions, B. Perthame, and P. Souganidis. Existence of entropy solutions to isentropic gas dynamics system. *Comm. Pure Appl. Math.*, 49:599–638, 1996.
- [45] P.-L. Lions, B. Perthame, and E. Tadmor. Kinetic formulation of the isentropic gas dynamics and  $p$ -systems. *Commun. Math. Physics*, 163:415–431, 1994.
- [46] O. Nwogu. Alternative form of Boussinesq equations for nearshore wave propagation. *Journal of Waterway, Port, Coastal and Ocean Engineering, ASCE*, 119(6):618–638, 1993.
- [47] D. Peregrine. Long waves on a beach. *J. Fluid Mech.*, 27:815–827, 1967.
- [48] O. Pironneau. *Méthodes des éléments finis pour les fluides*. Masson, 1988.
- [49] R. Rannacher. On Chorin’s projection method for the incompressible Navier-Stokes equations. In G. Heywood, John, K. Masuda, R. Rautmann, and A. Solonnikov, Vsevolod, editors, *The Navier-Stokes Equations II — Theory and Numerical Methods*, volume 1530 of *Lecture Notes in Mathematics*, pages 167–183. Springer Berlin Heidelberg, 1992.
- [50] W. C. Thacker. Some exact solutions to the non-linear shallow-water wave equations. *J. Fluid Mech.*, 107:499–508, 1981.
- [51] M. Vallée, R. Grandin, S. Ruiz, B. Delouis, C. Vigny, E. Rivera, E.-M. Aissaoui, S. Allgeyer, Q. Blétery, C. Satriano, N. Poiata, P. Bernard, J.-P. Vilotte, and B. Schurr. Complex rupture of an apparently simple asperity during the 2014/04/01 Pisagua earthquake (Northern Chile, Mw=8.1). In *EGU General Assembly Conference Abstracts*, volume 18 of *EGU General Assembly Conference Abstracts*, page 8660, Apr. 2016.

## A Equivalence with the Green-Naghdi system

In this section, we prove the equivalence up to some second order error terms between the formulation (1)-(5) and the Green-Naghdi system described in [39, 14, 40] i.e. we generalise [42] to the 2d case and with a non flat topography.

Following the formulation given in [40, paragraph 2.1] (see also [14]), the Green-Naghdi system writes

$$\frac{\partial H}{\partial t} + \nabla_{x,y} \cdot (HU) = 0, \quad (103)$$

$$(1 + \mu \mathcal{T}[H, z_b]) \left( \frac{\partial U}{\partial t} + (U \cdot \nabla_{x,y})U \right) + g \nabla_{x,y} (H + z_b) + \mu \mathcal{Q}[H, z_b]U = 0, \quad (104)$$

with  $U = (u, v)$  and

$$\begin{aligned} \mathcal{T}[h, z]W &= \mathcal{R}_1[h, z](\nabla_{x,y} \cdot W) + \beta \mathcal{R}_2[h, z](\nabla_{x,y} z \cdot W), \\ \mathcal{Q}[h, z]W &= -2\mathcal{R}_1[h, z](\partial_x W \cdot \partial_y W^\perp + (\nabla_{x,y} \cdot W)^2) + \beta \mathcal{R}_2[h, z](W \cdot (W \cdot \nabla_{x,y}) \nabla_{x,y} z), \end{aligned}$$

where  $W^\perp = (-W_2, W_1)^T$  if  $W = (W_1, W_2)^T$  and

$$\begin{aligned} \mathcal{R}_1[h, z]f &= -\frac{1}{3h} \nabla_{x,y} (h^3 f) - \beta \frac{h}{2} f \nabla_{x,y} z, \\ \mathcal{R}_2[h, z]f &= \frac{1}{2h} \nabla_{x,y} (h^2 f) + \beta f \nabla_{x,y} z. \end{aligned} \quad (105)$$

Notice that in the previous equations and as in [40, paragraph 2.1], the parameter  $\mu$  corresponds to the shallowness of the flow while  $\beta$  accounts for the amplitude of the topography variations.

The two models (1)-(5) and (103)-(104) correspond to shallow water flows and hence are mainly valid in the context of  $\mu, \beta \ll 1$ . The following proposition holds.

**Proposition A.1** *Up to  $\mathcal{O}(\mu\beta^2)$  terms, the model (1)-(5) with  $\gamma = 3/2$  and the model (103)-(104) are equivalent.*

**Corollary A.1** *Considering a modified Green-Naghdi model where the definition of  $\mathcal{R}_2[h, z]$  is slightly modified and becomes*

$$\tilde{\mathcal{R}}_2[h, z]f = \frac{1}{2h} \nabla_{x,y} (h^2 f) + \frac{3\beta}{4} f \nabla_{x,y} z,$$

*then the models (1)-(5) with  $\gamma = 3/2$  and the models (103)-(104) have exactly the same formulation.*

**Proof of prop. A.1** *The proof of the proposition is very simple in the sense that it only relies on simple computations but these computations are very long.*

*The dispersive terms in the Green-Naghdi model (103)-(104) i.e. the complementary terms compared to the classical shallow water system writes*

$$\mathcal{P}_{gn} = \mu \mathcal{T}[H, z_b] \left( \frac{\partial U}{\partial t} + (U \cdot \nabla_{x,y})U \right) + \mu \mathcal{Q}[H, z_b]U,$$

*whereas, for the model (1)-(4) their expression is given by (for  $\gamma = 3/2$ )*

$$\mathcal{P} = \mu (\nabla_{x,y} (Hp) + 3\beta p \nabla_{x,y} z_b), \quad (106)$$



with  $p$  defined by

$$p = \frac{2H}{3} \left( \frac{\partial w}{\partial t} + \mathbf{u} \cdot \nabla_0 w \right), \quad (107)$$

and  $w$  satisfies

$$\frac{3}{2}w = -H\nabla_0 \cdot \mathbf{u} + \frac{3\beta}{2} \mathbf{u} \cdot \nabla_0 z_b. \quad (108)$$

In order to prove the result it remains to insert the expression of  $w$  given by Eq. (108) into Eq. (107) then to insert the obtained expression for  $p$  into Eq. (106) and finally to check that  $\mathcal{P} - \mathcal{P}_{gn} = \mathcal{O}(\mu\beta^2)$  holds true.

Notice that in order to be consistent with the model formulation (103)-(104), in Eq. (106) the value of  $\mathcal{P}$  is multiplied by the shallowness parameter  $\mu$  and the gradient of the topography  $\nabla_0 z_b$  is multiplied by  $\beta$  in Eqs. (106),(108).

Since they can be easily carried out using any symbolic computation software, we do not reproduce the details of the computations allowing to obtain the simplified expression for the quantity  $\mathcal{P} - \mathcal{P}_{gn}$  corresponding to

$$\mathcal{P} - \mathcal{P}_{gn} = \frac{\mu\beta^2}{4} \left( \nabla_{x,y} z_b \cdot \left( \frac{\partial U}{\partial t} + (U \cdot \nabla_{x,y}) U \right) \right) \nabla_{x,y} z_b + \frac{\mu\beta^2}{4} (U \cdot (U \cdot \nabla_{x,y}) \nabla_{x,y} z_b) \nabla_{x,y} z_b. \quad (109)$$

■

**Proof of corollary. A.1** The proof is very simple to obtain since it is a direct consequence of the obtained expression for  $\mathcal{P} - \mathcal{P}_{gn}$  in Eq. (109) since we can rewrite

$$\begin{aligned} \mathcal{P} - \mathcal{P}_{gn} = \mu\beta(\mathcal{R}_2[H, z_b] - \tilde{\mathcal{R}}_2[H, z_b]) & \left( \nabla_{x,y} z_b \cdot \left( \frac{\partial U}{\partial t} + (U \cdot \nabla_{x,y}) U \right) \right) \\ & + \mu\beta(\mathcal{R}_2[H, z_b] - \tilde{\mathcal{R}}_2[H, z_b]) (U \cdot (U \cdot \nabla_{x,y}) \nabla_{x,y} z_b). \end{aligned}$$

■